Nanoparticle Notch Filters for Selective Filtering of Blue Light in Contact Lenses

by

Harish Krishnakumar

A thesis

presented to the University of Waterloo

in fulfilment of the

thesis requirement for the degree of

Master of Applied Science

in

Chemical Engineering (Nanotechnology)

Waterloo, Ontario, Canada, 2018

Author’s Declaration

This thesis consists of material all of which I authored or co-authored: see Statement of Contributions included in the thesis. This is a true copy of the thesis, including any required final revisions, as accepted by my examiners.

I understand that my thesis may be made electronically available to the public.

Statement of Contributions

I would also like to state the contributions of Andrew Bright, Vyshna Krishakumar, Fezza Haider, Shannon Tsai and Kashyap Kartha in synthesizing nanoparticles for many of my experiments, and conducting some experiments of my behalf. In this they all contribute to chapters 3 to 4.

The concepts, planning, parameter setting, experimental work, and analysis are my own.

Abstract

The visible wavelengths are essential to a normal colour vision, however overexposure of high-energy visible (HEV) light may be damaging to both ocular and non-ocular health. Some health concerns associated with HEV light (commonly referred to as blue light) include retinal damage, age-related macular degeneration (AMD) and photophobia in benign essential blepharospasm (BEB) and migraine patients. Certain wavelengths of blue light are essential to regulating bodily functions such as pupillary light reflex, melatonin regulation, and circadian rhythm, therefore completely filtering out these wavelengths may have adverse health effects. Despite its health impact, there is a severe dearth of blue light filtering eyewear that provide adequate protection from harmful blue-light wavelengths while allowing beneficial wavelengths of blue light to be transmitted.

Contact lenses are an attractive platform for incorporating blue-light filters. There are currently over 71 million contact lens wearers worldwide, however there are currently no commercially available contact lenses on the market offering both UV and blue light protection.

This thesis presents a novel approach to selectively filtering out blue-light wavelengths in contact lenses through the use of plasmonic silver nanoparticles (AgNPs). First, a tunable synthesis process was developed to allow for the production of AgNPs with customizable localized surface plasmon resonance (LSPR) peaks between 400 – 450 nm and full width at half maximum (FWHM) values of less than 45 nm. Next, the blue-light filtering AgNPs were encapsulated with a thick, uniform layer of silica to preserve colloidal and optical stability as well as minimizing leaching of Ag^+ ions. Lastly, the silica-coated AgNPs were integrated into commercial etafilcon contact lenses using industry transferrable processes. The NP-integrated lenses demonstrated blue-light filtering capabilities while being transparent in the visible wavelengths. In addition, the NP-integrated

lenses demonstrate stability post-autoclaving, UV and natural sunlight exposure, and room temperature storage.

Acknowledgments

First, I would like to thank my supervisor Dr. Frank Gu for his guidance and support on this project. He provided me with a great opportunity to improve upon my research, problem-solving and communication skills through leading a challenging and highly-motivating project.

I would also like to thank the co-op students who worked with me: Andrew Bright, Vyshna Krishnakumar, Fezza Haider, Shannon Tsai and Kashyap Kartha. In addition, I would like to thank Michelle Si for her assistance with autoclaving samples.

Major funding for this work comes from Johnson and Johnson Vision Care, the University of Waterloo, and the National Sciences and Engineering Research Council of Canada. I would also like to thank Kevin McCabe and Charles Scales for their feedback throughout this project.

Dedication

To my mother and father.

Table of Contents

List of Figures

List of Tables

List of Equations

List of Abbreviations

In order of appearance

HEV: high-energy visible

AMD: age-related macular degeneration

BEB: benign essential blepharospasm

UV: ultra-violet

AgNPs: silver nanoparticles

SPR: surface plasmon resonance

LSPR: localized surface plasmon resonance

FWHM: full width at half maximum

IR: infrared

RPE: retinal pigment epithelial

ROS: reactive oxidative species

ipRGCs: intrinsically photosensitive retinal ganglion cells

A2E: N-retinylidene-N-retinylethanolamine

NPs: nanoparticles

MDI: Millipore deionized water

OD: optical density

TEM: transmission electron microscopy

ICP (ICP-OES): Ion conductive optical emission spectroscopy

Chapter 1. Introduction

1.1. Background

Although the visible wavelengths are essential to a normal colour vision, there is growing concern that overexposure of high-energy visible (HEV) light may be damaging to both ocular and non-ocular health. HEV light (commonly referred to as blue light) includes violet, blue and blue-green light which corresponds to 380 – 500 nm on the electromagnetic spectrum [1, 2]. Some blue light exposure is essential to regulate functions within the human body such as circadian rhythm, melatonin regulation, and pupillary light reflex, though overexposure may disrupt these functions [3, 4]. Other concerns associated with blue light include retinal damage, age-related macular degeneration (AMD), and photophobia in migraine and benign essential blepharospasm (BEB) patients [5, 6, 7, 8, 9]. Blue-light filtering may also be beneficial to improve vision, including increased visual acuity and glare reduction [4, 10].

With over 71 million users worldwide, contact lenses are an attractive platform for incorporating blue light filters [11]. Despite several patents being issued, there are currently no commercially available contact lenses on the market offering both UV and blue light protection [12, 13, 14, 15].

Plasmonic materials, such as silver nanoparticles (AgNPs), present a novel and promising approach to selective filtering of blue light wavelengths in contact lenses while overcoming some of the limitations of using blue light absorbing dyes. Plasmonic nanoparticles are ideal for light filtering applications because the absorbance and scattering properties can be tuned by making subtle changes to the particle shape and size [16, 17, 18]. In contrast, the chemical formula of commercial pigments and dyes must be modified to change the light absorbing and scattering properties. In addition, the surface of silver nanoparticles (AgNPs) is easily modified by polymers through specific electrostatic interactions or by thiol functionalization, allowing for stable dispersion in a variety of matrices [19]. These material properties support the integration of transparent AgNPs into contact lenses to produce blue light absorbing lenses (as seen in Figure 1).

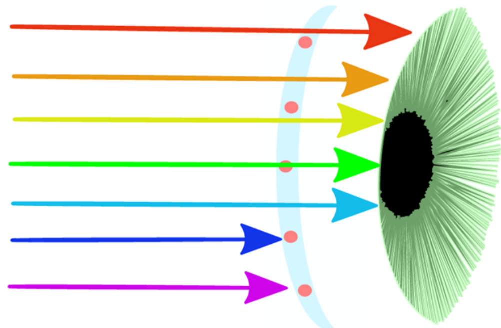

Figure 1. Illustration of AgNP (pink spheres) integrated lenses filtering out harmful high-energy wavelengths and allowing transmission of lower energy wavelengths.

1.2. Research objectives

The goal of this research was to develop transparent nanoparticles that are capable of filtering specific wavelengths of blue light and are designed to interface with contact lens materials and industrial manufacturing processes. This was done by addressing the following research objectives:

(1) Developing a tunable synthesis process that allows for the production of plasmonic silver nanoparticles with customizable localized surface plasmon resonance (LSPR) peaks between 400 – 450 nm and full width at half maximum (FWHM) values of less than 45 nm (to minimize the amount of beneficial visible light that is filtered out).

(2) Depositing a thick, uniform layer of silica around individual AgNPs to preserve the colloidal and optical stability of the plasmonic cores and minimize leaching of Ag^+ ions.

(3) Integrating the silica-coated AgNPs into etafilcon hydrogels through photocuring and then demonstrating stability post-autoclaving, UV and natural sunlight exposure, and room temperature storage.

1.3. Thesis outline

This thesis is written as follows:

Chapter 1 serves as an outline for the research presented. It provides an overview of the thesis itself, along with background information.

Chapter 2 is an in-depth literature review, split into two main sections. Section 1 highlights the ocular and non-ocular health effects associated with blue light exposure, the potential benefits to selectively filtering out harmful blue light wavelengths, and the current limitations in eyewear providing protection from blue light wavelengths. Section 2 focuses on the properties of plasmonic nanoparticles and their potential to be applied as selective blue light filters in contact lenses.

Chapter 3 discusses the first phase in development of blue light filtering contact lenses, which is to develop a protocol that can be used to produce silver nanoparticles with tunable LSPR peaks throughout the region of harmful blue light wavelengths (400 – 450 nm). The polyol synthesis was tuned such that the concentration of Cl^- ions in the reaction medium could be used to selectively synthesize cubic or octahedra nanoparticles in a one-pot synthesis. Under these optimized conditions the LSPR of the nanoparticles can be red-shifted over a range of ~40 nm, without significantly compromising transparency in the visible wavelengths. In addition, the synthesized nanoparticles are shown to have far superior optical properties in comparison to commercially available silver nanoparticles.

Chapter 4 demonstrates the first steps towards transferring the optimized optical properties of the cubic and octahedra AgNPs in Chapter 3 into materials with practical commercial applications. The AgNPs were successfully silica-coated, resulting in a protective layer around the plasmonic cores that improves both colloidal and optical stability. In addition, the silica coating is shown to be an effective tool to further tune the LSPR of the synthesized AgNPs without compromising transparency in the visible wavelengths. Silica-coated AgNPs were integrated into etafilcon contact lenses using industry transferrable methods, where the nanoparticles were introduced into etafilcon monomer mixture and photocured under blue light. The silica-coated AgNPs were able to successfully impart blue light filtering capabilities on commercial etafilcon contact lenses without hindering the transparency in the visible region. In addition, the NP-integrated lenses show stability under autoclaving, UV and solar exposure as well as minimal leaching of silver ions and nanoparticles during storage.

Chapter 5 wraps up the research with conclusions and suggestions for future work.

Chapter 2. Literature Review

2.1. Introduction

The human eye is adapted to radiation emitted by the sun [20]. Our vision is based on the absorption of light by photoreceptors within the eye; through this process our eyes use light to obtain information about our surroundings [20, 21]. Although the visible wavelengths are essential to a normal colour vision, there is growing concern that overexposure of high-energy visible (HEV) light may be damaging to both ocular and non-ocular health. HEV light (commonly referred to as blue light) includes violet, blue, and blue-green light which correlates to 380 – 500 nm on the electromagnetic spectrum. Unlike UV light (100 nm to 380 nm) blue light is not completely filtered out by the cornea and crystalline lens, allowing it to pass through to the retina [1, 2]. This makes wavelengths between 380 – 500 nm the highest-energy photons to be absorbed by the retinal structures, and as a result there is concern about the impact of HEV light in this region. In addition, the rampant increase over the last decade in blue light exposure from digital devices such as smartphones and computer monitors has led to growing concerns about the health impact of blue light. Overexposure may disrupt circadian rhythm, melatonin regulation, and pupillary light reflex [3, 4]. Blue light exposure has also been linked to age-related macular degeneration (AMD), and photophobia in migraine and benign essential blepharospasm (BEB) patients [5, 6, 7, 8, 9]. Blue-light filtering may also be beneficial to improve vision, including increased visual acuity and glare reduction [4, 10]. The following sections will focus on the ocular and non-ocular health effects associated with blue-light exposure, the benefits to selectively filtering blue light, and commercially available blue light filters.

2.2. Interaction of light with structures in the eye

When sunlight interacts with the eye, wavelengths of light are absorbed by different tissues and molecules within the eye. The wavelengths that are transmitted to the retina are essential for colour perception and regulating circadian rhythm.

2.2.1. **Cornea**

The human cornea absorbs all UVC light (100-280 nm). It also effectively absorbs UVB radiation (280-315 nm) and approximately 30-40% of UVA light (315-380 nm). The cornea is also effective at absorbing infrared radiation (780 nm to 1 mm) [22].

2.2.2. **Lens**

The lens in the adult human eye is an effective filter for UVB, UVA and some infrared (IR) wavelengths. The transmission profile of the human lens changes with age. With aging, the lens absorbs more blue light. Young children are at higher risk of damage from blue light exposure, seeing as only 35% of blue light is filtered by their lenses [1].

2.2.3. **Retina**

The wavelengths that reach the retina include the visible wavelengths (380-780 nm) and some near IR wavelengths [22, 23]. There are two main classes of photoreceptors in the retina that mediate vision, rod and cone. Rod photoreceptors are responsible for vision at low light levels (scotopic vision). They have high sensitivity but lack colour information, and their peak absorption is at 507-530 nm. Rhodopsin is the visual pigment found in rod photoreceptors [1, 24]. Cone photoreceptors mediate photopic vision and are responsible for colour vision. *In vivo*, the peak absorbance of the three different cone photoreceptors are around 450 nm for blue cones, 540 nm for green cones and 570 nm for red cones [1].

The third class of photoreceptors are called intrinsically photosensitive retinal ganglion cells (ipRGCs). IpRGCs contain the photopigment melanopsin, which has an action spectrum that peaks around 480 nm [25]. The light-responsive ipRGCs regulate many non-visual physiological functions in the body. These functions include circadian entrainment, pupillary light reflex, and melatonin regulation [26, 27]. The various photoreceptors in the retina are summarized in Table 1.

Table 1. Photoreceptors in the retina.

Photoreceptor	Photopigment	Peak Wavelength (nm) in Mammalian Cells	Function
Rods	Rhodopsin	507	Responsible for scotopic vision.
Short-wavelength cones	Cyanolabe	450	Responsible for photopic vision.
Medium-wavelength cones	Chlorolabe	540	
Long-wavelength cones	Erythrolabe	570	
ipRGCs	Melanopsin	480	Regulate many non-visual physiological functions including circadian entrainment, pupillary light reflex, and melatonin regulation.

2.3. Retinal damage and AMD

The primary health concern associated with blue light is AMD. AMD is a leading cause of blindness among seniors over the age of 65 [28, 29]. Even more concerning is that the global AMD population is expected to grow between 100-200 million people over the next 3 decades [4].

In vivo studies on primates have revealed retinal damage associated with blue light is due to cumulative photochemical damage [5, 6]. Exposure to light between 380 – 500 nm results in the photoactivation of all-*trans*-retinal accumulated in the photoreceptor outer segments, which induces the production of reactive oxygen species (ROS) such as hydrogen peroxide, free radicals, and singlet oxygen [30]. ROS are known to attack polyunsaturated fatty acids (a key component of cell membranes) and as the retina has many cell membranes, the eye is rendered highly sensitive to oxidative stress. The resulting oxidative stress interferes with the membrane structures of photoreceptor outer segments and causes the incomplete phagocytosis of oxidized outer segments of retinal pigment epithelial (RPE) cells. Overall, the process results in the accumulation of waste known as lipofuscin in RPE cells [4].

Lipofuscin build-up is a significant contributor to AMD development. Lipofuscin typically accumulates as a person ages, however blue light exposure can accelerate the process [31]. Lipofuscin's phototoxicity is mediated by the photosensitive fluorophore A2E (N-retinylidene-N-retinylethanolamine). A2E is excited by blue light wavelengths with a peak absorption at 440 nm [30]. The photosensitization of lipofuscin leads to further ROS formation and inhibits lysosomal activity [32, 33].

The excess oxidative stress resulting from A2E photosensitization and lipofuscin accumulation eventually leads to RPE apoptosis. Once the RPE cells die, photoreceptors will also degenerate [4]. In addition to lipofuscin accumulation, aging also results in a decrease in the retinal concentrations of macular pigments [34, 35, 36]. Macular pigments such as lutein and zeaxanthin are natural protective filters that attenuate blue light wavelengths before they reach the RPE and photoreceptors. Lutein has a peak absorbance at 452 nm and zeaxanthin has a maximal absorbance at 463 nm [37]. Aside from filtering HEV light, macular pigments also act as free-radical scavengers [38].

There are limited treatment options available for patients with AMD. In the 1980s, laser photocoagulation showed some effect in reducing long-term severe visual loss, but this was coupled with minimal vision gain and high recurrence rates [39, 40]. Photodynamic therapy with verteporfin was introduced in the 1980s. The therapy consists of two-stages. The first stage involves intravenous infusion of verteporfin, which preferentially accumulates in neovascular membranes. The dye is then activated with infrared light. When the dye is activated, it generates oxygen-free radicals that damage the endothelium and promote the closure of newly formed vessels. Photodynamic therapy is rarely used for age-related macular degeneration now. Some patient groups that had received photodynamic therapy reported adverse effects, including photosensitivity, headaches, and acute vision loss [41].

With the dearth of effective treatment options, AMD prevention is the most prudent option and may be achieved through selective filtering of blue light wavelengths. In 2008, researchers at the Paris Vision Institute identified the wavelengths from 415 – 455 nm as the most phototoxic region of blue light [37]. The researchers split the visible light spectrum between 380 nm and 500 nm into multiple 10 nm bands and studied the effect on A2E-containing porcine RPE cells exposed by these wavelengths. The researchers found that apoptotic cell death was both A2E-dose dependent and wavelength dependent, with wavelengths centered near 440 nm resulting in a significant increase in apoptosis.

2.4. Circadian rhythm

The circadian rhythm is an evolutionary feature that allows organisms to synchronize their physiological processes to the time of day [42, 43]. Studies have shown that blue light is the most significant environmental cue to entrain mammalian circadian rhythm [3]. The photoreceptors involved in circadian entrainment are knowns as ipRGCs, and these photoreceptors contain the photopigment melanopsin which has a maximal absorption at 480 nm [25]. Melanopsin has been implicated in regulating pupillary light reflex, circadian entrainment, and melatonin regulation [3]. In a study conducted on mice, it was found that melanopsin-knockout mice showed incomplete pupillary light reflex at high irradiances [44]. Tests on humans have found that melatonin suppression has a peak absorbance around 460 nm, which suggests melanopsin plays a key role in regulating melatonin levels [45]. Melatonin secretion is associated with increased sleep propensity, and as a result, inhibiting melatonin secretion implicates the natural sleep cycle [46]. Several studies have shown that blue light wavelengths between 440 nm to 480 nm are effective in shifting the human circadian clock and disrupting regular sleep patterns [47, 48, 49]. Individuals that experience sleep deficiency may experience several adverse health effects including a greater risk of obesity, heart disease, diabetes, stroke, and depression [50].

Despite the adverse effects of overexposure of blue wavelengths near 460 nm on circadian entrainment, filtering out all blue light wavelengths may also be detrimental to physiological functions regulated by ipRGCs. Several studies have shown that pupillary constriction is wavelength dependent and peaks at 480 nm, which is the maximal absorption of ipRGCs [27, 51, 52]. Pupil constriction is the eye's natural defense to strong light exposure. In addition, Ishikawa et al. found that filtering out light at 470 nm could disrupt the sustained phase of the pupil constriction reflex [53]. Clearly, some blue light exposure is necessary for regulating circadian entrainment, however overexposure of blue light wavelengths near 460 nm should be minimized (especially at night) to avoid disrupting the circadian clock.

2.5. Blue light induced photophobia

Photophobia is an abnormal sensitivity to light and it is often associated with several neurological disorders including migraines and benign essential blepharospasm [54, 55]. Recent studies reveal ipRGCs play a key role in the physiological processes associated with photophobia [56, 57]. These findings support the numerous studies which reveal blue light wavelengths seem to have the most harmful effects on patients afflicted with photophobia [7, 8, 9].

2.5.1. **Mechanism/Pathway**

IpRGCs act as transducers, converting light into a pain stimulus [56, 58]. Upon photoactivation, these melanopsin-containing cells direct their response towards thalmic pain centers [56]. There is some belief in the scientific community that the pathway between ipRGCs and the thalmic pain centers may have a pathologic gain among patients with certain neurologic disorders [55]. Unlike rod and cone photopigments, melanopsin is a biphasic photopigment, where photoactivation drives both processes of phototransduction and pigment regeneration [51, 59]. Recent data suggests melanopsin can be photoconverted between the 11-cis and all-trans isoforms through exposure to blue light (~480 nm) and orange-red light (590-620 nm) [59, 60]. The 11-cis isoform is maximally sensitive to blue light wavelengths at 480 nm, whereas the 11-cis isoform has a peak sensitivity at longer wavelengths (590-620 nm) [51, 60]. Under ambient light settings, the existence of two stable photon absorption states allows melanopsin to be continuously photoconverted between the dual states, which in turn results in photic responses being directed towards the thalmic pain centers.

2.5.2. **Migraines**

Migraines are the most common neurological disorder, affecting roughly 6% of men and 18% of women [61]. Almost all migraine patients report light sensitivity [62]. Studies have shown that blocking wavelengths near 480 nm reduce light sensitivity among those with migraines [9, 57]. Good et al. showed that children wearing blue-green light blocking FL-41 tinted spectacle lenses experienced a drop in migraine frequency from 6.2 to 1.6 per month [9]. Hoggan et al. found that patients wearing spectacles with a thin film optical notch filter centered at 480 nm reported improved daily functionality [57].

2.5.3. **Benign essential blepharospasm**

Benign essential blepharospasm (BEB) is a disorder characterized by excessive and involuntary spasms of the eyelids [63]. BEB is a severely debilitating condition, and in some cases it may render the patient functionally blind [64]. As with migraine-sufferers, most BEB patients also report light sensitivity [65]. Blackburn et al. showed that BEB patients wearing FL-41 tinted lenses experienced reduced light sensitivity and blink frequency [66]. FL-41 has a maximal absorbance peak around 480 nm, similar to the action spectrum of melanopsin [55].

2.6. Visual acuity and glare

In addition to preserving ocular and non-ocular health, there is considerable interest in blocking blue light wavelengths to improve visual performance. Blue light filters are popular among athletes and sharpshooters who believe the filters reduce glare and improve visual acuity [4, 67]. The improvement in vision resulting from filtering high-energy blue light wavelengths may be due to UV and blue light being scattered by the atmosphere at a greater propensity than longer-wavelength light [4]. In addition, glaring may be caused by UV and blue light wavelengths photo-activating the crystalline lens to weakly fluoresce [68]. Despite the popularity of blue light filters among those demanding sharp vision, there is little scientific evidence to support these claims [67].

Filtering blue light wavelengths near the UV region may be beneficial to patients with ocular conditions that result in clouding of the ocular media [10]. Intraocular light scattering is reportedly higher in individuals with aphakia, albinism, and cataracts [10, 69]. By filtering blue light wavelengths near the UV region, light scattering in ocular media can be decreased [70, 71, 72]. Rosenblum et al. found wearing blue light filters with a 50% transmission peak centered around 445 nm improved visual acuity by 19% and contrast sensitivity function by 27% among aphakic individuals [10].

Individuals with dry eye disease may also benefit from wearing eyewear with blue light filtering capabilities. Dry eye disease is characterized by corneal opacity and persistent dryness of the conjunctiva [73]. Kaido et al. showed that dry eye patients had a significant improvement in visual acuity while wearing eyeglasses that blocked 50% of blue light [74].

2.7. Development of notch filters for selective filtering of blue light wavelengths

Due to blue light wavelengths being both beneficial and detrimental, it is challenging to develop blue light filters that improve human health. Filters that block off most or all blue light wavelengths may be visually unappealing due to their strong yellow colour. They may also have unwarranted effects such as distortion of colour perception and disruption of circadian entrainment. To limit the possibilities of causing adverse health effects, notch filters that selectively filter specific wavelengths of blue light (see Table 2) should be considered.

Table 2. Notch filters by wavelengths.

Wavelength(s) (nm)	Beneficial Effect to Filtering Wavelengths
380-420	May reduce glare and improve visual acuity in aphakic and dry eye patients.
415-455	These wavelengths have been identified as the most phototoxic wavelengths to RPE cells. Blocking these wavelengths may prevent development of AMD.
460	460 nm is the peak absorbance of melatonin suppression. Filtering out wavelengths near 460 nm at night may help preserve circadian rhythm.
480	480 nm is the peak absorbance wavelength of ipRGCS. Filtering out wavelengths near 480 nm may reduce light sensitivity for migraine-sufferers and BEB patients who experience photophobia.

Such filters are difficult to design due to their sharp drop-offs in transmission at specific wavelengths, but some promising patents for designing optical notch filters in the blue light region have been filed (as seen in Table 3). Metal plasmonic nanoparticles have been considered given the optical properties of these materials are tunable in the blue light region [75]. Hoggan et al. designed a notch filter centered around 480 nm through sequential deposition of thin layers of metal oxides onto substrate lenses [57]. The optical properties of the lenses were tuned by controlling the composition, thickness, and ordering of the metal oxide layers [55]. Blue light absorbing dyes and pigments with narrow absorption bandwidths have also been proposed as notch filters integrated into spectacles and/or contact lenses [76].

Table 3. Patents describing the application of selective blue light notch filters in eyewear.

Patent Name	Number	Assignee	Method of Selective Filtering	Application
Nanoparticle light filtering method and apparatus	US20150168616A1	University of Utah Research Foundation	Plasmonic nanoparticles	Reducing severity of photophobic responses, (including migraine headache and blepharospasm) or for regulating circadian cycles [75].
Tinted polarized lenses having selective frequency filtering	US9891448B2	Smith Optics Inc	Polarized film coating	Reducing glare and improving colour perception [76].
Circadian rhythm optical film	US20150268396A1	3M Innovative Properties Co	Polymeric interference filters	Reduce circadian rhythm disruption [77].
High performance selective light wavelength filtering providing improved contrast sensitivity	US8360574B2	High Performance Optics	Blue light absorbing pigment or dye	Improve contrast sensitivity [78].
High energy visible light filter systems with yellowness index values	US8882267B2	High Performance Optics	Blue light absorbing dye	One potential application of this invention is that it may reduce cell death due to limiting exposure by wavelengths near 430 nm [79].
Rugate optical lens to prevent macular degeneration	US20060092374A1	High Performance Optics	Rugate filter	To provide protection against macular degeneration [80].

2.8. Commercially available blue light filters

2.8.1. **Spectacles**

There are several commercially available spectacle lenses that offer blue light protection. These lenses typically use blue light absorbing materials or surface coatings to reduce the transmission of blue light wavelengths [81]. Despite the abundance of blue light filtering spectacles on the market, these lenses have not been widely accepted by society. The limiting factors for widespread usage of blue light filtering spectacles include that (1) they may be cosmetically unappealing because of a yellow or amber tint produced by blocking of blue light wavelengths, (2) the yellow or amber tint imparted on the spectacles may interfere with normal colour perception and (3) it is difficult to selectively filter out harmful wavelengths of blue light while allowing the essential blue light wavelengths to pass through [78, 81].

Essilor addressed many of the limiting factors with their blue light filtering spectacles, “Crizal Prevencia No-Glare”. These lenses selectively filter out harmful UV and blue light wavelengths (between 415 to 455 nm). They also reduce the transmission of blue light wavelengths between 415 to 455 nm by 20% while causing minimal colour distortion – appearing almost completely clear [4]. In vitro studies conducted with A2E-containing RPE cells demonstrated the efficacy of the lenses as they were able to reduce cell apoptosis by 25% compared to no light filtering whatsoever [37]. Leung et al. studied the performance of several commercially available blue light filtering spectacles, including “Stressfree” and “Noflex” from SwissLens, on computer users over the course of a month. Both spectacle lenses were measured to have transmittance less than 0.2% in the UV and near UV region. “Stressfree” blocked 17.8% blue light through anti-reflective coating whereas the brown-tinted “Noflex” was measured to block 22.5% of blue light. Wearers reported no significant change in sleep quality, contrast sensitivity and glare while wearing the blue-light filtering spectacle lenses [81]. Spectacles such as “Noflex” and “Stressfree” may be an option for protecting the eye from harmful blue light without adversely affecting visual performance and circadian rhythm. However, it is unclear whether the low levels of blue light blockage (17.8 – 22.5%) in these lenses is sufficient for preventing development of AMD and other harmful health effects.

2.8.2. **Contact lenses**

Contact lenses are an attractive platform for incorporating blue light filters. There are currently over 71 million people worldwide using contact lenses for vision correction, therapeutic and cosmetic purposes [11, 82]. Unlike sunglasses, where UV and HEV light can still reach the eyes through the top, bottom and sides of the glasses, contact lenses can provide complete protection from light at all angles since they cover the entire cornea [83, 84, 85]. There are several contact lenses on the market, most notably the Acuvue brand offering “Class 1” UV protection (blocking >90% UVA and >99% UVB) [86, 87]. Despite several patents being issued, there are currently no commercially available contact lenses on the market offering both UV and blue light protection [12, 13, 14, 15].

Most of these blue light filtering contact lens patents describe methods of incorporating blue light-absorbing molecules that are copolymerized with the polymer(s) used to manufacture the lenses. This is to eliminate potential leaching of blue-light absorbing molecules. There are several challenges with incorporating blue light filtering molecules into contact lenses:

(1) Contact lenses are most commonly fabricated using cast molding in the industry, and this typically involves curing the polymers under UV (or HEV light) to form the lens. The blue light absorbing dye may absorb the curing light, resulting in a longer cure or

requiring increased light intensity. This may also result in the final properties of the lens being compromised [88].

(2) The blue light absorbing agent may affect the kinetics of polymerization especially if a significant amount of the agent is added to the monomer mixture [88].

(3) If the blue light absorber needs to be copolymerized with the lens matrix, it limits the choice of materials available for blue light blocking in lens [88].

(4) The polymerized lens (containing the blue light absorbing agent) must be able to withstand sterilization conditions and be stable in the contact lens packing solution [89].

2.9. Nanoparticles for notch filters

2.9.1. Overview of nanoparticles

Nanomaterials refers to objects with dimensions in the range of 1 – 100 nanometers, approximately the size of 10 – 1000 atoms. At the nanoscale, well-known materials can take on new properties due to quantum effects. Small enough nanoparticles (~ half the wavelength of light), will cease to scatter light that they do not absorb, making the material appear transparent [90]. By tuning the light absorption of nanoparticles and taking advantage of sizes that avoid light scattering, blue light blocking nanoparticles can be developed with the potential to be applied as spectral filters in contact lenses.

Semiconducting NPs such as TiO_2 and ZnO are frequently used in sunscreens as inorganic UV blockers [90]. By using nanoscale TiO_2 and ZnO, the undesired opaqueness of the materials is eliminated while still providing sufficient UV protection [90]. Materials engineering allows for the preparation of doped TiO_2 for control over band structuring (e.g. nitrogen or metal-doped TiO_2) to increase the amount of visible blue light that is absorbed. However, it is difficult to achieve selective filtering of blue-light wavelengths over a narrow region, as doping tends to increase the amount of light that is absorbed over a broad region of visible light [91, 92, 93].

Quantum dots exhibit remarkable and tunable optical properties. In addition, low-cost synthesis methods with high degree of control over material properties exist [94, 95, 96]. However, there are concerns over the toxicity of quantum dots [97]. In addition, quantum dots are well known for their intense fluorescent properties, which is undesirable in a contact lens.

Plasmonic nanoparticles, such as silver and gold, are very promising materials for blue light blocking applications and contact lens integration. Plasmonic nanoparticles are ideal for light absorbing applications because the absorbance and scattering properties can be tuned by making subtle changes to the particle shape and size [16, 17, 18]. In contrast, the chemical formula of commercial pigments and dyes must be modified to change the light absorbing and scattering properties. This significantly reduces the tunability of pigments. Silver is an ideal candidate for blue light blocking and contact lens integration. The surface of silver nanoparticles (AgNPs) is easily modified by polymers through specific electrostatic interactions or by thiol functionalization, allowing for stable dispersion in a variety of matrices [19]. Furthermore, silver enjoys application in a wide range of consumer goods including food and personal care products. While recent literature strongly recommends careful consideration toward toxicity of all nanomaterial-containing products, using materials already approved for consumer goods helps ensure the safety of the product [98]. These material properties support the integration of transparent AgNPs with contact lenses to produce blue-light absorbing lenses while mitigating health and approval risks associated with new products.

2.9.2. **Plasmonic nanoparticles and LSPR**

Metallic nanoparticles made of silver and gold have generated significant interest for research and commercial applications due to their unique optical properties. Silver and gold nanoparticles are now considered as inorganic chromophores with strong extinction [99]. These metallic nanoparticles can display very intense colours when dispersed in liquid media due to surface plasmon resonance (SPR), which corresponds to the frequency of oscillation at which conductive electrons oscillate due to the electrical field of the incident electromagnetic radiation [99, 100].

The intense light absorbing and scattering properties of metallic nanoparticles have been actively considered for use as nanoscale devices for enhanced light scattering in solar cells, photon energy transport, surface-enhanced Raman/fluorescence scattering, and chemical/biological sensing. Many of these applications require the SPR band to be tunable over a broad range [99]. The only metallic materials to exhibit plasmonic effects in the visible spectrum are gold, silver and copper NPs. The SPR peak of metal nanostructures includes both absorption and scattering components, and unlike in bulk materials, these components are dependent on the size, shape, surrounding media, and composition of the nanostructure [16, 17, 18]. In the case of metal nanoparticles, the collective oscillation of free electrons is confined to a finite volume, and the corresponding plasmon is referred to as a LSPR [100]. In a sense, the surface plasmons are electromagnetic waves trapped at the dielectric/metal interface due to the collective oscillations of free electrons in the metal [100]. This phenomenon was explained by Gustov Mie in 1908 [101]. Mie theory can be used to determine the extinction cross-section of spherical nanoparticles at a given size as seen in Equation 1 [102]:

$$C_{ext} = \frac{24\pi^2 R^3 \varepsilon_m^{3/2}}{\lambda}\left[\frac{\varepsilon_i}{(\varepsilon_\tau + 2\varepsilon_m)^2 + \varepsilon_i^2}\right]$$

Equation 1: Extinction coefficient determination using Mie theory.

where C_{ext} is the extinction cross section, λ is the excitation wavelength, R is the particle radius, ε_m is the relative dielectric constant of the medium around the NP, and ε_τ and ε_i are the real and imaginary parts of the dielectric function, respectively. However, there are several limitations of Mie theory. Mie theory only applies to the optical properties of a single, isolated nanoparticle in a homogenous environment. In addition, Mie theory is unable to account for non-spherical shapes, coating and shell layers, or the effects of nanoparticle aggregation [103].

To overcome the limitations of Mie theory, several other approximation techniques can be used to determine the optical properties of non-spherical nanoparticles, such as dipole, quadrupole, and discrete dipole approximation (DDA) [103]. This thesis will not include numerical methods and modelling to determine the optical properties of synthesized plasmonic materials. All optical values reported in this thesis are determined from experimental data.

2.9.3. **Tuning the optical properties of silver**

Among the various plasmonic metal NPs, AgNPs show the greatest promise for light filtering applications due to their high surface plasmon strength and tunability of the SPR absorption spectra from 300 to 1200 nm. The surface plasmon strength is described using the quality factor (Q) described in Equation 2 [102]:

$$Q = \frac{w(d\varepsilon_r/dw)}{2\varepsilon_i^2}$$

Equation 2. Quality factor

The surface plasmon strength is directly proportional to the quality factor. Large Q values indicate strong plasmons whereas a low Q indicates weak surface plasmons with a small C_{ext}. Low quality factors are also correlated with broadening of the extinction spectra FWHM [104]. In comparison to other plasmonic metals, silver has the largest quality factor across most of the spectrum from 300 to 1200 nm. In addition, interband transitions involving excitations of electrons from the conduction to higher energy levels also contribute to dampening the surface plasmon modes [105]. In silver, these interband transitions take place at much higher frequencies than the LSPRs, however in the case of gold and copper, these interband transitions limit their LSPR excitations to wavelengths above 500 and 600 nm, respectively [106]. It is for these reasons that silver appears as an ideal candidate for selective filtering of blue light wavelengths.

The LSPR of silver nanoparticles can be tuned by controlling the size, shape, surrounding media, and elemental composition [16, 17, 18]. The size of the AgNPs can be modulated to shift the SPR absorption peak. Increasing the size of the nanoparticles will red-shift the SPR, but also broaden the absorption band. The effect of scattering also becomes more dominant at larger sizes [107, 108].

The SPR of AgNPs can also be significantly altered by changing the shapes of the NPs. NPs with sharper features will have a more red-shifted SPR in comparison to spherical nanoparticles and nanoparticles with rounded corners [109]. This is due to the sharp features of the AgNPs increasing the charge separation and reducing the restoring force for the dipole oscillation [110]. Small spherical AgNPs (less than 20 nm in size) typically have one SPR around 400 nm in water [111]. In comparison, cubic, octahedra and right bipyramids will have one strong SPR peak at a more red-shifted wavelength along with multiple shoulders at more blue-shifted wavelengths. The number of SPR peaks increases with non-spherical shapes due to a loss in symmetry. This leads to polarization of electrons in multiple directions. Shape control can be a very effective way to tune the SPR of AgNPs throughout the blue light regions. Changing the shape of the nanoparticles from spheres to cubes, octahedra, and right bipyramids, can red-shift the SPR peak by up to 40, 50 and 100 nm, respectively [110]. The added advantage of this tunability is that the overall size of the NPs is not significantly increased, and so broadening of the extinction spectra can be minimized.

The LSPR of the AgNPs can also be tuned by modulating the dielectric constant of the surrounding medium. By coating AgNPs with dielectric materials such SiO_2 or TiO_2, the LSPR can be red-shifted throughout the visible spectrum [112].

2.9.4. **Silica coating**

There has been a great deal of interest over the last two decades in encapsulating individual plasmonic NPs in silica shells [113]. The main driving force behind this interest is that bare plasmonic nanoparticles are poorly suited for the harsh conditions required for many applications. Without a protective coating, the optical properties of plasmonic nanoparticles may be compromised due to particle aggregation, etching, or reshaping [114]. Silica coating has emerged as a promising approach to improve the stability of plasmonic nanoparticles and facilitate their integration into sensors, as well as catalytic, biomedical, and photovoltaic devices [115, 116].

In contact lenses, the motivation behind coating plasmonic nanoparticles with silica can be categorized into 4 functions: (1) improving colloidal stabilization, (2) protecting the cores from the surrounding medium, (3) attaining a higher degree of control over the optical properties in harsh environments, and (4) functionalizing and integrating the nanoparticles into a contact lens (Table 4).

Silica shells improve colloidal stabilization against aggregation through electrostatic and steric repulsion. The exposed silanol groups allow for free cations to adsorb onto silica surfaces, leading to long-range electrostatic repulsion between nanoparticles [116]. Steric repulsion arises at short interparticle distance due to the comparatively lower Hamaker constant of silica in water ($A_{silica} = 1 \times 10^{-20}$ J vs $A_{Ag} = 1\text{-}4 \times 10^{-19}$ J) which leads to weaker van der Waals interactions [117, 118]. The synergistic effects of electrostatic and steric stabilization have been to show to prevent irreversible aggregation, even in solvents with high ionic strengths [119, 120]. In addition, silica coating imparts greater mechanical stability which can prevent morphological changes and fixate specific particle structures [121, 122].

Silica coating has also been shown to inhibit the oxidative etching of less noble metals such as silver. Furthermore, silica coating can reduce the toxicity of the plasmonic metal nanoparticle by preventing leakage of ions from the cores [123, 124].

Silica coating can also be used to tune and control the optical properties of plasmonic nanoparticles. The deposition of a silica layer usually causes the LSPR to red-shift due to the increase in the refractive index surrounding the plasmonic core [114]. If a sufficiently thick silica layer is deposited on the nanoparticles, it can act as a spacer layer that prevents plasmons from interacting with adjacent NPs. The LSPR of plasmonic nanoparticles usually red-shift in response to particle aggregation, however, the introduction of a silica spacer layer effectively separates adjacent plasmonic cores and prevents coupling of their electric fields [125, 126]. This is illustrated in Figure 2.

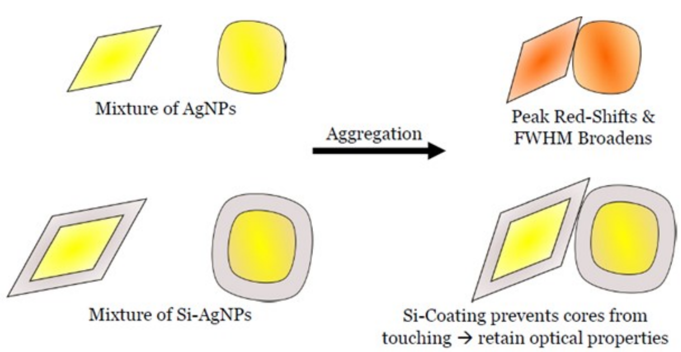

Figure 2. Schematic illustration depicting how optical properties are preserved due to silica acting as a spacer layer between plasmonic nanoparticles in close proximity.

Aside from optical tuning, silica coating may also be desirable from a material compatibility/integration perspective. The presence of exposed silanol and siloxane groups on the silica shell allow for further functionalization that may facilitate lens integration and long-term stability [127]. Silane coupling chemistry may be applied to functionalize the nanoparticles with reactive agents that can cross-link the plasmonic materials into the contact lens matrix under photocuring. Or alternatively, the silica shell can be functionalized to improve the stability and dispersion of the NPs in various monomer mixtures.

In summary, the potential to improve surface functionalization, colloidal and chemical stabilization, and further tune optical properties of plasmonic materials make the silica shell a high desirable feature in designing AgNP based blue light filtering contact lenses. The potential functions of the silica shell are summarized in Table 4.

Table 4. Potential functions of silica shell in plasmonic blue light filters in contact lenses.

Function	Description	References
Colloidal Stabilization	Prevent irreversible aggregation. Fixate the shape of NP structures.	[119, 120, 121, 122]
Chemical Stabilization	Protect plasmonic cores from oxidative etching.	[123, 124]
Optical Properties Tunability	Redshift the LSPR to a desired wavelength. Minimize changes in optical properties due to NP aggregation.	[125, 126]
Surface Functionalization and Integration	Functionalize the NPs with reactive agents that can cross-link into the contact lens.	

Chapter 3. Silver nanoparticle synthesis

3.1. Introduction

There are a wide array of chemical synthesis protocols available for preparing silver nanoparticles of various sizes and shapes, including citrate and silver mirror reduction, polyol process, seed-mediated growth and light-mediated synthesis [128, 129, 130, 131, 132]. For applications such as sensing and selective light filtering, it is critical to attain nanoparticles of uniform size and shape. The polyol process is a simple and versatile method that has been used to make silver nanoparticles of various shapes, including cubes, rods, wires, and octahedra [133, 134, 135]. However, synthesis of AgNPs through the polyol process has been plagued by reproducibility issues stemming from trace impurities and poor temperature control [102]. In addition, controlling the reduction and growth rates are essential to synthesizing nanoparticles within an appropriate time frame. Long synthesis periods extending past several hours are inconvenient from a production perspective, however short synthesis times (less than 15 minutes) are also undesirable due to difficulties in being able to effectively monitor the reaction and quench it once a specific size/shape of nanoparticles has been obtained. Previous reports of cubic AgNP synthesis using the polyol process show the ability to tune the LSPR from ~400 nm to wavelengths near 500 nm [133, 134, 135]. In addition, Xia et al. reported FWHM values as narrow as 30 nm for LSPR peaks between 401 to 418 nm [133]. However, narrow FWHM values for LSPRs at more red-shifted wavelengths (420-450 nm) have not been reported with AgNPs. In this chapter we demonstrate reproducible AgNP synthesis of cubic and octahedra structures by simply tuning the salt concentration in the polyol process. To the best of our knowledge this is the first reported demonstration of tuning the concentration of NaCl to selectively synthesize cubic or octahedra AgNPs in a one-step polyol synthesis. In addition, the experimental parameters of the synthesis have been tuned such that (1) the NP synthesis can be monitored and quenched over an appropriate time phase (45-120 minutes) and (2) narrow FWHMs (< 45-50 nm) can be attained at LSPRs > 440 nm. The ability to synthesize AgNPs with narrow FWHMs for LSPRs between 400-450 nm is crucial to developing a library of selective blue light filters.

3.2. Materials and methods

3.2.1. **Materials**

Ethylene glycol (EG, 99.8%), silver trifluoroacetate (CF_3COOAg, ≥99.99%), poly(vinylpyrrolidone) (PVP, MW ≈ 55, 000), sodium chloride (NaCl) and sodium hydrosulfide hydrate ($NaHS$-xH_2O) were purchased from Sigma-Aldrich. All chemicals were used as received. The synthesis of AgNPs was carried out in 20 mL glass scintillation vials, purchased from VWR. A filtration device was purchased from EMD Millipore to produce Millipore-grade water (>15 MΩ.cm).

All glassware was cleaned prior to use with 12 M NaOH for 1 hour followed by washing with copious amounts of DI water, and 3 washes of Millipore-grade water. Stir bars were cleaned with nitric acid for 10 minutes, followed by washing with copious amount of Millipore-grade water.

40 nm (cat no. 795968) and 60 nm (cat no. 795984) spherical, PVP functionalized AgNPs were purchased from Sigma-Aldrich for comparison purposes. Optical properties of commercial AgNPs were measured in-house. TEM sizing information of commercial AgNPs reported in this thesis are based off of the supplier's information.

3.2.2. **Synthesis of AgNP**

Synthesis of cubic AgNPs. The synthesis of cubic AgNPs was based off a modified polyol synthesis [136]. 5 mL of EG was added to a 20 mL scintillation vial and heated in an oil bath set at a temperature between 115 – 130 °C. The temperature was monitored throughout the entirety of the synthesis. All reagents were dissolved in EG and sequentially added to the scintillation vial placed in the oil bath. 90 µl of NaSH (3 mM) was first introduced, followed by PVP (20 g/L) and NaCl (1.5 mM) after a 2-minute delay. Lastly, 0.4 mL of CF_3COOAg (282 mM) was introduced after 2 minutes. The scintillation vial was loosely capped, and aliquots were taken at 15-minute intervals with a glass Pasteur pipette. All aliquots were diluted with Millipore deionized water (MDI) prior to TEM and UV-Vis analysis.

Synthesis of octahedra AgNPs. The synthesis parameters of octahedra AgNPs were identical to that of cubic AgNPs except for the concentration of NaCl. 0.5 mL of 0.075 mM NaCl was added to the scintillation vial to prepare octahedra AgNPs.

3.2.3. **Characterization**

NP optical density (OD) spectra were obtained with a UV-Vis spectrophotometer (BioTek Epoch). The size and shape of the particles were analyzed with a Philips CM-10 transmission electron microscope (TEM). Particle diameters were measured using ImageJ software. The average diameter and standard deviations were calculated using built-in function on Microsoft Excel. Large, irregularly shaped NPs were excluded from the analysis.

3.3. Results & Discussion

3.3.1. **Influence of Cl^- ions**

Cubic AgNPs were prepared following the synthesis protocol in Section 3.2.2 (with the temperature set at 130 °C). Under these experimental conditions, the growth kinetics were slow enough such that the LSPR could be easily monitored throughout the synthesis. After 90 minutes the AgNPs had attained a LSPR peak of 430 nm with a FWHM of 47 nm as seen in Figure 3.

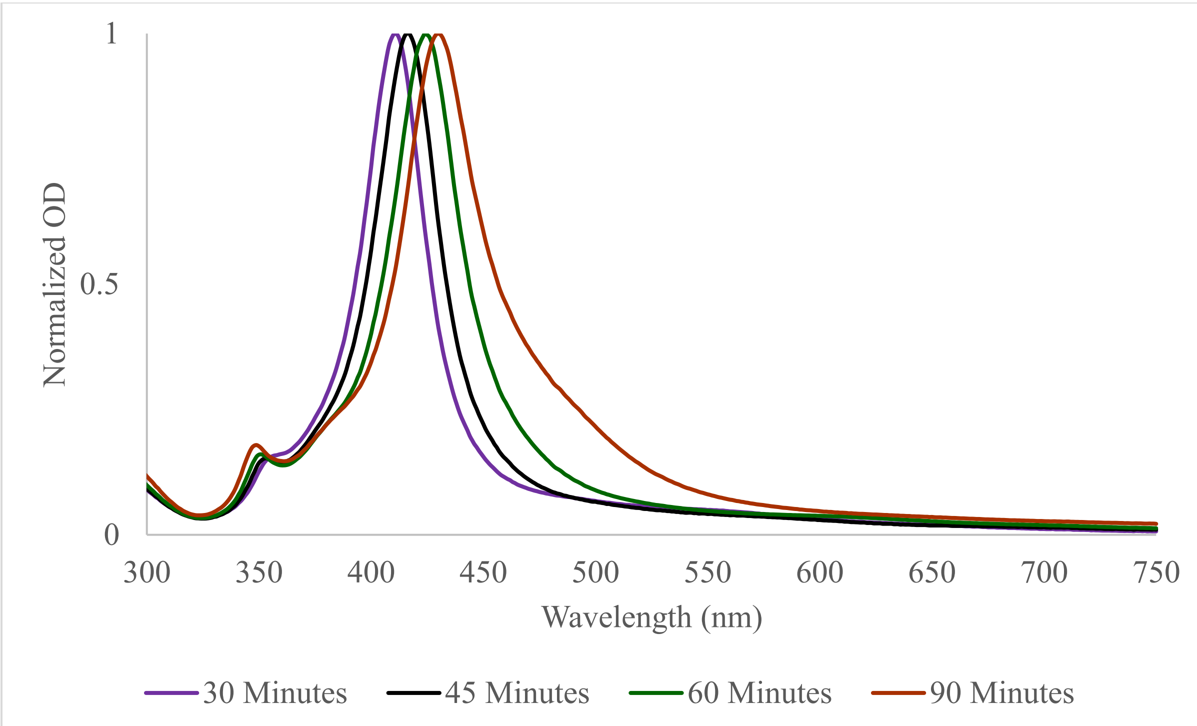

Figure 3. Normalized OD spectra of aliquots obtained at different time points during the synthesis of cubic AgNPs.

The progression of nanoparticle growth was also studied under TEM analysis as seen in Figure 4. 30 minutes into the synthesis, the nanoparticles appear to be quasi-spherical in shape with an LSPR peak at 411 nm. At the 45-minute timepoint, the nanoparticles are larger, and this is accompanied by a red-shift in the LSPR of ~5 nm. At this stage, the nanoparticles appear to be cuboctahedra with an average diameter of 33.1±5.9 nm. Well-defined cubic nanoparticles with sharp corners are finally attained after 90 minutes. In addition, the average particle diameter increased to 42.1±5.9 nm. The changes in the optical properties include both a significant red-shift in the LSPR and the development of a well-defined shoulder peak at ~347 nm. This shoulder peak is associated with cubic AgNPs [137]. The cubic morphology arises due to a high yield of single crystal seeds attained during the initial stages of the reaction, shape-directed growth by PVP, and oxidative etching (assisted by Cl^- ions) to eliminate twinned and multi-twinned particles [134, 138].

PVP acts as a shape directing agent by preferentially binding to the {100} facets, thereby lowering their free energy. In the absence of PVP, the {111} facets have the lowest free energies of Ag polyhedrons followed by the {100} and {110} facets. [11] Cubic nanoparticles are enclosed by {100} facets, therefore PVP is required to lower the free energy of these facets.

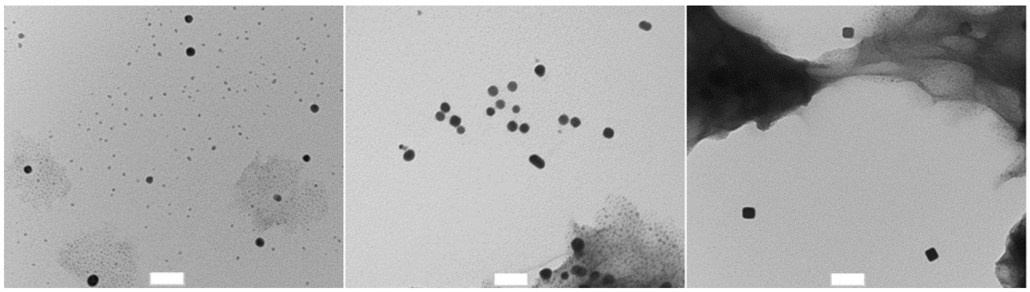

Figure 4. TEM images of aliquots obtained during the synthesis of cubic AgNPs after 30 (left), 45 (middle) and 90 (right) minutes. Scale bar represents 100 nm.

Throughout the reaction, there was a very low percentage of right bipyramids and irregular shapes. This is partly due to the role of chloride and oxygen in controlling the growth of single crystal seeds in the early stages of nanoparticle growth. The oxidative etching mechanism outlined by previous works suggests that the combination of an oxidant (such as oxygen) and a ligand (such as chloride) is capable of not only coordinating to metal ions in the reaction solution, but to also act as etchants for both seeds and nuclei [134, 138]. Out of the three most dominant crystalline structures taken on by metal seeds, single-crystal structures are far more resistant to oxidative etching than twinned and multi-twinned structures. Twinned and multi-twinned structures contain a greater amount of defect regions that are higher in activity and hence more susceptible to oxidative etching [134]. Chloride was used to great effect in this process to eliminate the presence of twinned and multi-twinned structures during the early stages of the synthesis.

Lowering the concentration of NaCl by a factor of two led to the LSPRs being far more red-shifted but at the expense of the FWHM values of these LSPRs being broader (Figure 5). Apart from red-shifting the LSPR peaks, the lower salt concentration also resulted in the emergence of a 2nd shoulder peak around 380 nm after the 30-minute timepoint.

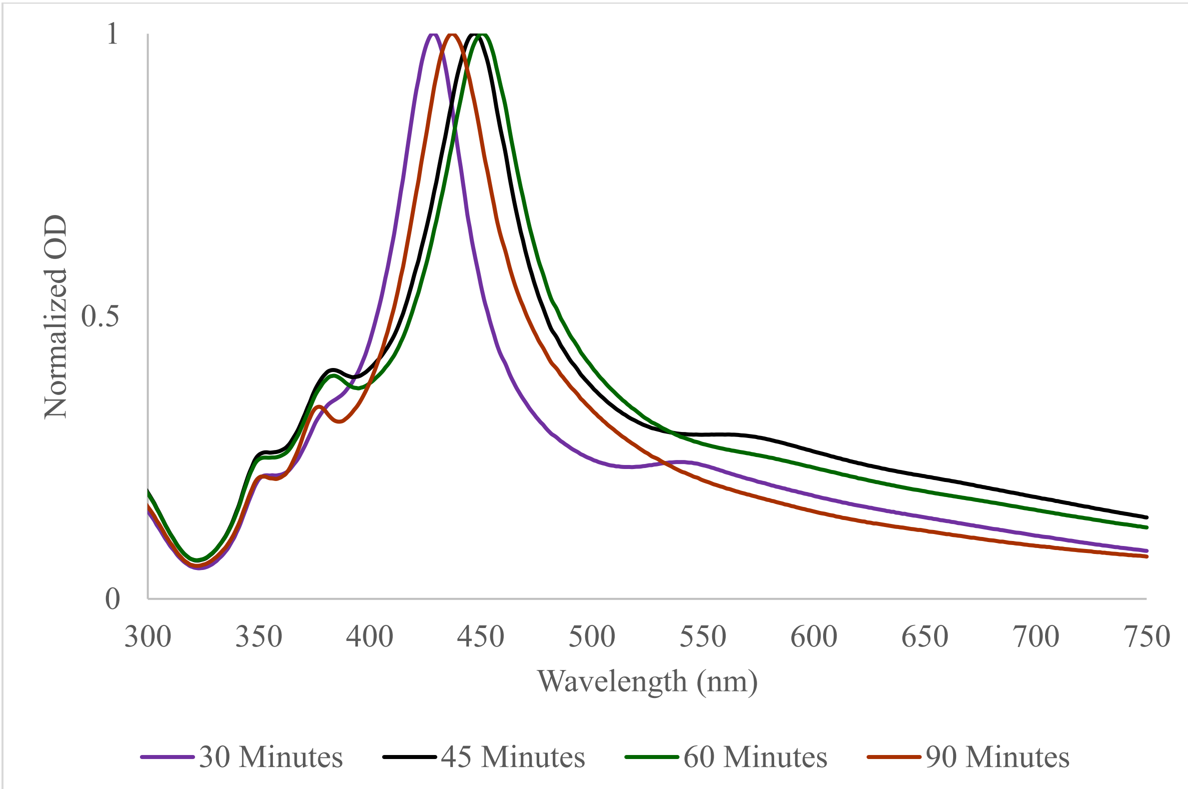

Figure 5 Normalized OD spectra of aliquots obtained at different timepoints during the synthesis of octahedra AgNPs.

The presence of these shoulder peaks indicates the presence of octahedra AgNPs [137]. TEM images taken after the 90-minute timepoint reveal the formation of octahedra AgNPs at the lower salt concentration (Figure 6). Under TEM analysis, the octahedra nanoparticles (Figure 6) are easily distinguishable from cubic nanoparticles (Figure 6) by their lack of perpendicular edges.

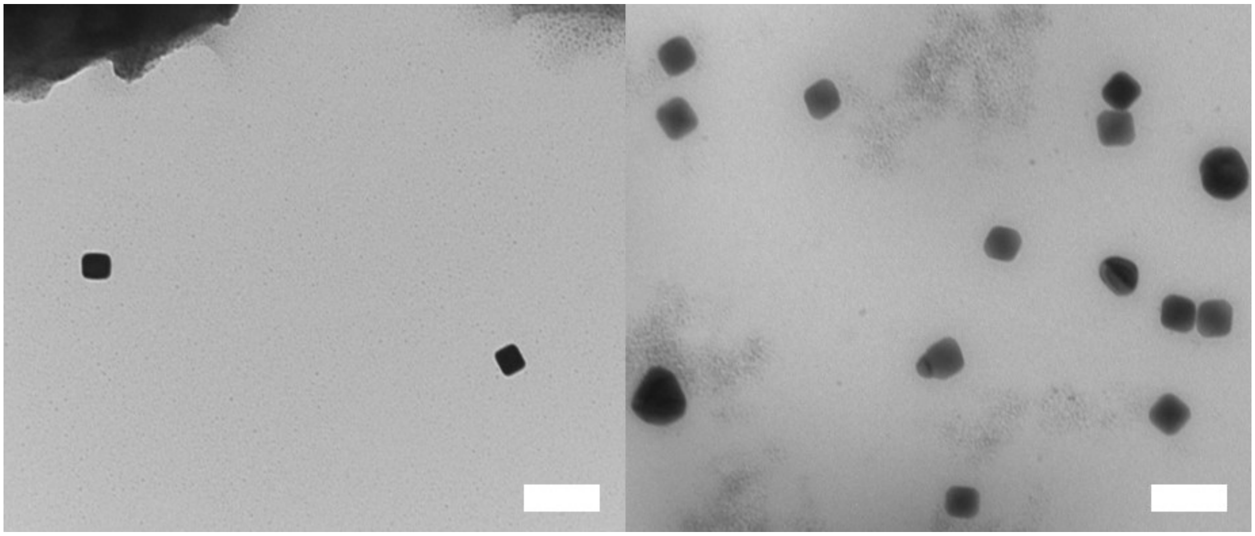

Figure 6. TEM images of cubes (left) and octahedra AgNPs (right) after 90 minutes of synthesis. Scalebar represents 100 nm.

Both octahedra and cubic nanoparticles stem from single crystal seeds. Preferential growth of either cubic or octahedra nanoparticles can be controlled by tuning the relative growth rates along the <111> and <100> directions. The formation of octahedra AgNPs by simply lowering the NaCl concentration suggests that the growth rate along the <100> direction is increased relative to growth along the <111> direction. To the best of our knowledge Cl^- and Na^+ ions have not been used to tune the relative growth rates of the <111> and <100> directions to synthesize AgNPs of cubic or octahedral shapes. Previously, PVP and sodium citrate have been used to direct the growth of cubes and octahedrons respectively in a two-step polyol process [137, 139]. Citrate ions preferentially bind to {111} facets whereas PVP strongly adheres to {100} facets, as previously mentioned.

These results suggest that Cl^- ions may also preferentially adhere to the {100} facets, and that it is the synergistic effect of PVP and Cl^- ions that direct the growth of cubic nanoparticles from single crystal seeds. It is interesting to note that at the lower Cl^- concentrations, single crystalline seeds were still the dominant species, however it should be noted that there does seem to be a slightly higher percentage of irregular shapes at this concentration (as seen in Figure 6).

This could be due to a reduction in oxidative etching of twinned and multi-twinned seeds during the early stages of the reaction, due to a lower availability of free Cl^- ions.

Comparing the progression of LSPR peaks of the nanoparticles synthesized at both salt concentrations reveals that the lower salt concentration led to much faster red-shifting of the LSPR peak (Table 5). However, the FWHM values of these LSPR peaks were broader and were accompanied by a shoulder peak at wavelengths > 500 nm. This indicates the presence of irregular nanoparticles [136]. Absorbance in this region is also undesirable for selective blue light filtering as it compromises the transparency in the visible light region.

Table 5. Change in LSPR (nm) over the course of the synthesis at low and high Cl^- concentrations.

Cl^- Concentration	Time (mins)				
	30	45	60	75	90
Low	429	447	451	449	437
High	411	416	424	431	430

The results from these syntheses are promising as they show the potential to develop a synthesis protocol that can produce AgNPs with tunable LSPR peaks > 435 nm and narrow FWHM values. The next steps involve controlling the growth kinetics of the reaction such that the LSPR can be red-shifted throughout the blue light region without compromising the FWHM and introducing undesirable shoulder peaks at wavelengths > 500 nm.

3.3.2. **Tuning the optical properties of octahedra AgNPs – NaHS variation**

Low concentrations of bisulfide (SH^-) are required to increase the reduction rate of the polyol synthesis such that cubic and octahedral AgNPs can be obtained within an adequate time frame [102]. Bisulfide is hypothesized to rapidly react with Ag^+ ions to form insoluble Ag_2S clusters which then serve as catalysts and seeds for rapid heterogenous nucleation of Ag atoms [136]. Table 6 shows the effects of varying the volume of NaHS added to the reaction while keeping all other parameters constant in the synthesis of octahedra AgNPs. Reducing the bisulfide concentration helped minimize the increase in the FWHM of the LSPR peak, however overall red-shifting of the peak was also significantly reduced.

Table 6. Evolution of LSPR peak and FWHM (denoted in brackets) at various NaHS volume additions.

Volume of NaHS (ul)	Time (min) 15	30	45	60	75	90
60	403 (34)	411 (28)	427 (34)	431 (37)	433 (38)	428 (38)
90	--	429 (50)	447 (64)	451 (66)	449 (61)	437 (61)
100	--	436 (99)	445 (68)	450 (82)	450 (88)	445 (78)

The growth of octahedral AgNPs at the reduced bisulfide concentrations was significantly slower. After 15 minutes into the reaction there is a single plasmon peak at 403 nm (as seen in Figure 7). A second plasmonic peak appears after 30 minutes, revealing the presence of cuboctahedra. A third plasmonic peak around 380 nm appears between 45 – 60 minutes into the reaction, indicating the formation of octahedra nanoparticles.

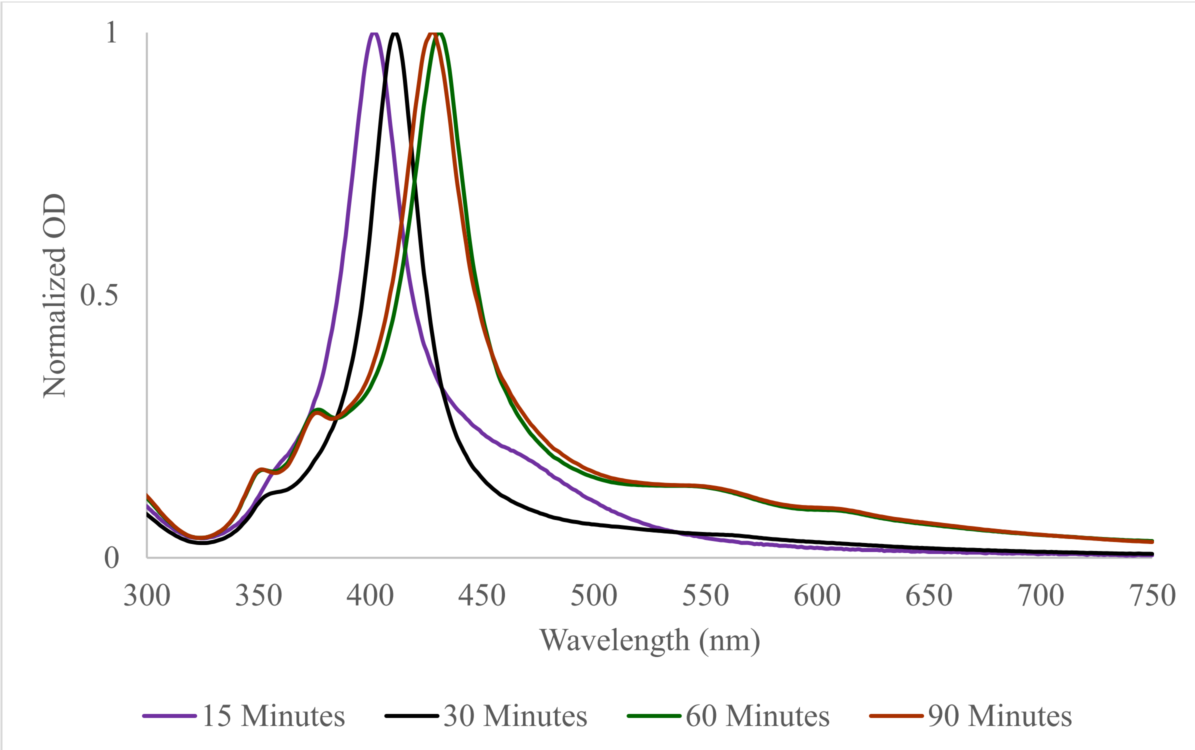

Figure 7. Normalized OD spectra of aliquots obtained at different timepoints during the synthesis of octahedra AgNPs (60 ul NaHS).

The results from the UV-Vis spectra correspond well with TEM images of the AgNPs at various stages of the reaction, as seen in Figure 8. Comparing the TEM images of AgNPs obtained at 15 and 30 minutes into the reaction, the key noticeable difference is in the size of the NPs. This difference in size contributes to a red-shift of 8 nm. Between 30 and 60 minutes, the NPs do not appear to be significantly larger, however the LSPR peak is red-shifted by 20 nm. This result shows that tuning the shapes and sharpness of features can be a powerful tool to tuning the LSPR of AgNPs. The controlled evolution of cuboctahedra to octahedra NPs allows for significant red-shifting without increasing the overall size of the NPs, thereby minimizing any broadening in the FWHM.

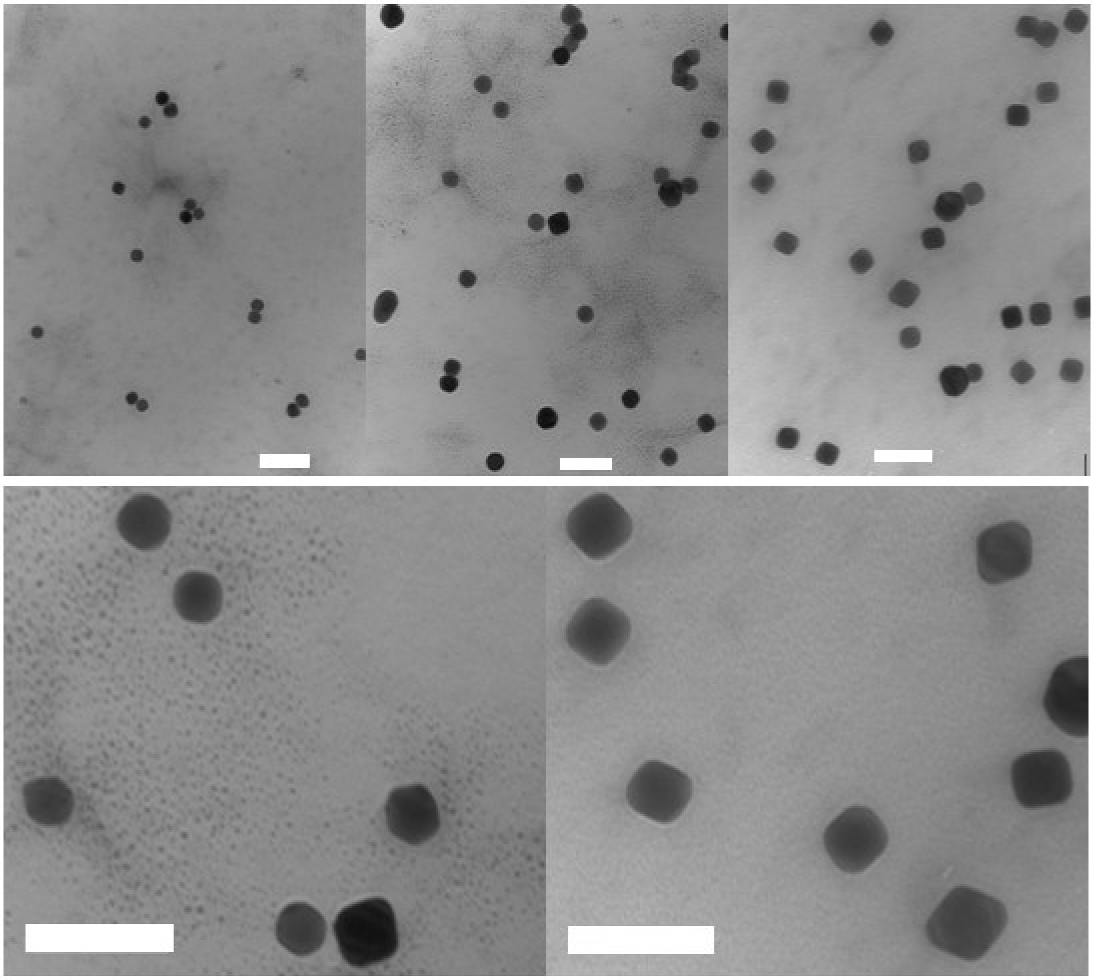

Figure 8. AgNP growth after 15 (top and bottom left), 30 (top middle) and 90 (top and bottom right) minutes into the synthesis. Scalebars represent 100 nm.

3.3.3. **Tuning the optical properties of octahedra AgNPs – Temperature variation**

The temperature of the reaction was also investigated as a parameter that can be tuned to slow down the growth kinetics. As seen in Table 7, reducing the synthesis temperature to 115 °C significantly reduced the rate of red-shifting of the LSPR peak. In spite of this reduced temperature, LSPR peaks >435 nm with narrow FWHM values (<40 nm) were attained, albeit over a longer period. The narrow FWHM values can be attributed to the high level of particle uniformity. Nearly 70% of the final product falls into a diameter range of 43-48 nm. The final product consists of monodisperse octahedra nanoparticles with an average diameter of 46.1±3.2 nm. A histogram showing the NP diameter distribution can be found in Appendix A.

Table 7. Evolution of octahedral AgNP LSPR peak and FWHM at various polyol synthesis temperatures.

Temperature (°C)	Time (min)						
	30	45	60	75	90	105	120
115	405 (29)	406 (28)	413 (30)	425-426 (36)	435 (34)	440 (35)	441 (35)
120	402-403 (44)	413-414 (32)	426 (36)	433 (34)	436 (33)	--	--
130	429 (50)	447 (64)	451 (66)	449 (61)	437 (61)	--	--

Under these optimized synthesis conditions, the LSPR was successfully red-shifted by 36 nm without compromising the FWHM of the LSPR peak, as depicted in Figure 9. These optimized synthesis conditions enable uniform nanoparticle growth, thereby allowing for the production of AgNPs with tunable, narrow LSPR peaks between 405 to 441 nm.

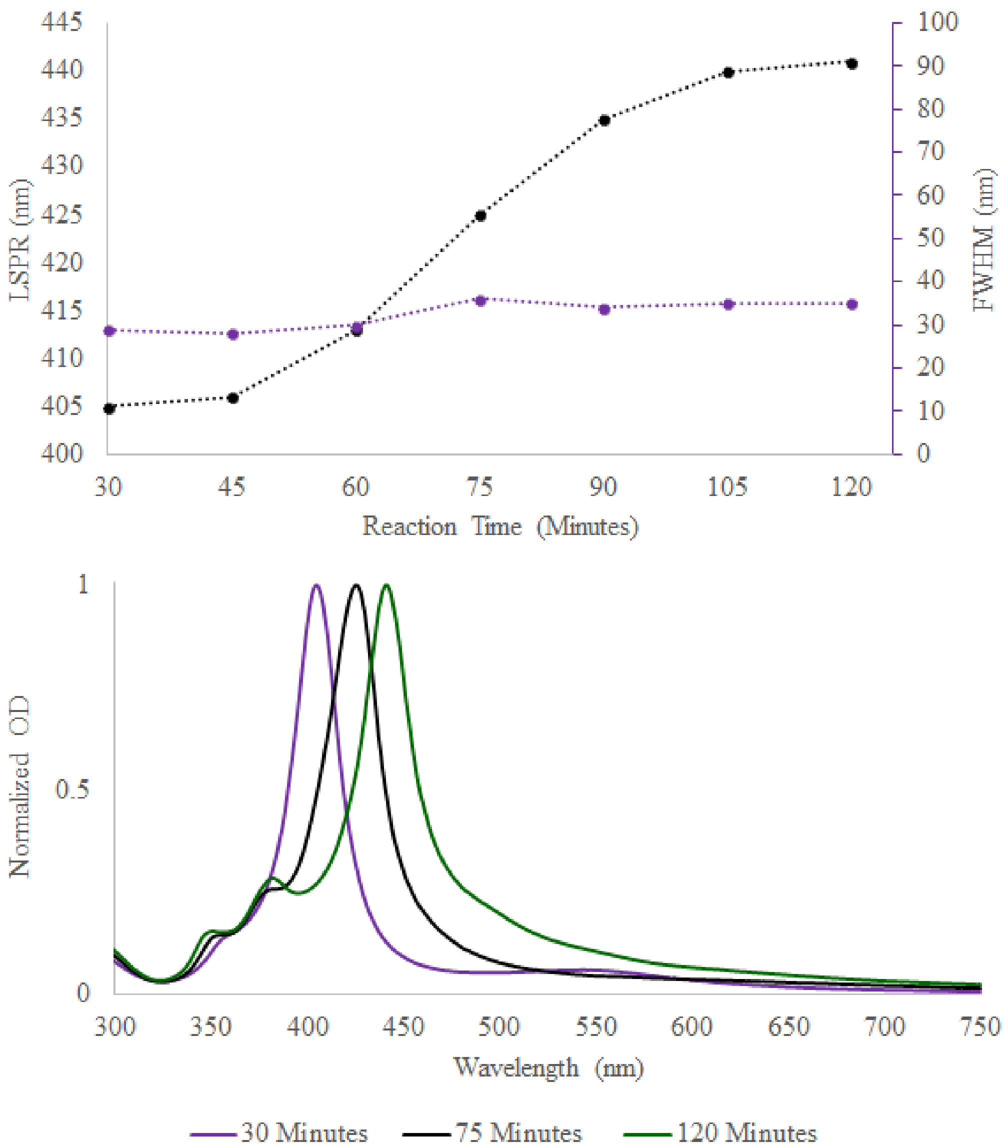

Figure 9. Evolution of LSPR and FWHM throughout the synthesis of octahedra AgNPs (top). Normalized OD spectra of aliquots obtained from the synthesis of octahedra AgNPS after 30, 75 and 120 minutes into the synthesis.

3.3.4. **Reproducibility**

Metal nanoparticle synthesis through the polyol method has been plagued by reproducibility issues due to a variety of factors [102]. Our optimized synthesis process for cubic and octahedral AgNPs (with the temperature set at 115 °C) is highly reproducible. The high reproducibility of our modified polyol process for octahedra AgNPs is shown in Table 8 (see Appendix B for cubic replicates and more replicates of octahedra AgNPs).

Table 8. Reproducibility of octahedra AgNPs under optimized polyol synthesis conditions.

	Time (min)						
	30	45	60	75	90	105	120
Replicate 1	405 (29)	406 (28)	413 (30)	425-426 (36)	435 (34)	440 (35)	441 (35)
Replicate 2	407 (30)	406 (28)	415 (32)	426 (36)	436 (36)	442 (36)	444 (37)
Replicate 3	408 (30)	407 (29)	416 (31)	427 (36)	438 (38)	441 (38)	444 (37)

3.3.5. **Comparing the optical properties of various shapes**

The optical properties of our cubic and octahedra AgNPs were compared to that of commercially available PVP-functionalized spherical AgNPs. 40 nm spherical AgNPs purchased from Sigma-Aldrich were measured to have an LSPR of 409 nm with a corresponding FWHM of 59 nm. As seen in Figure 10, octahedra and cubic AgNPs synthesized under our optimized synthesis conditions possess narrower LSPR peaks at much further red-shifted wavelengths, despite being comparable in size.

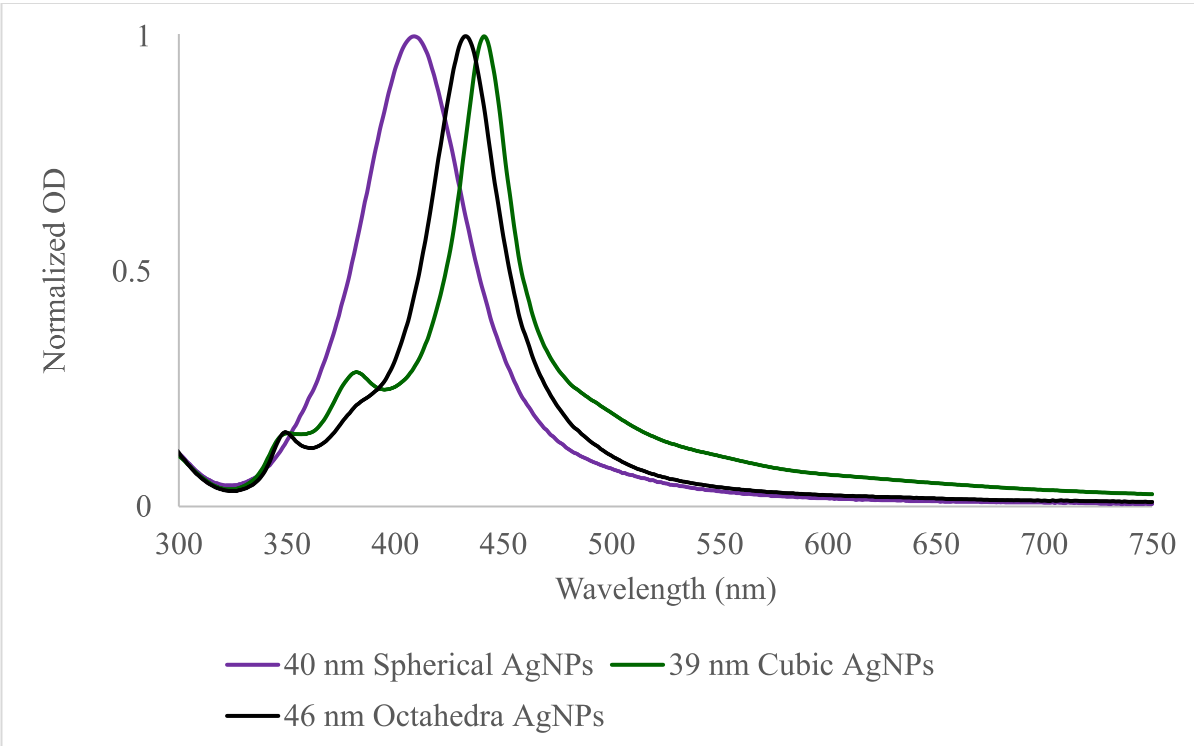

Figure 10. Normalized OD spectras of 40 nm commercial spherical AgNPs, cubic AgNPs and octahedra AgNPs.

Spherical AgNPs of 60 nm in diameter were measured to have an LSPR of 440-441 with a corresponding FWHM of 109 nm. The LSPR of these spherical AgNPs matches that of our 46.1±3.2 nm octahedra AgNPs (LSPR = 440 nm). However, as seen in Figure 11, the FWHM of the spherical AgNPs' LSPR is significantly broader.

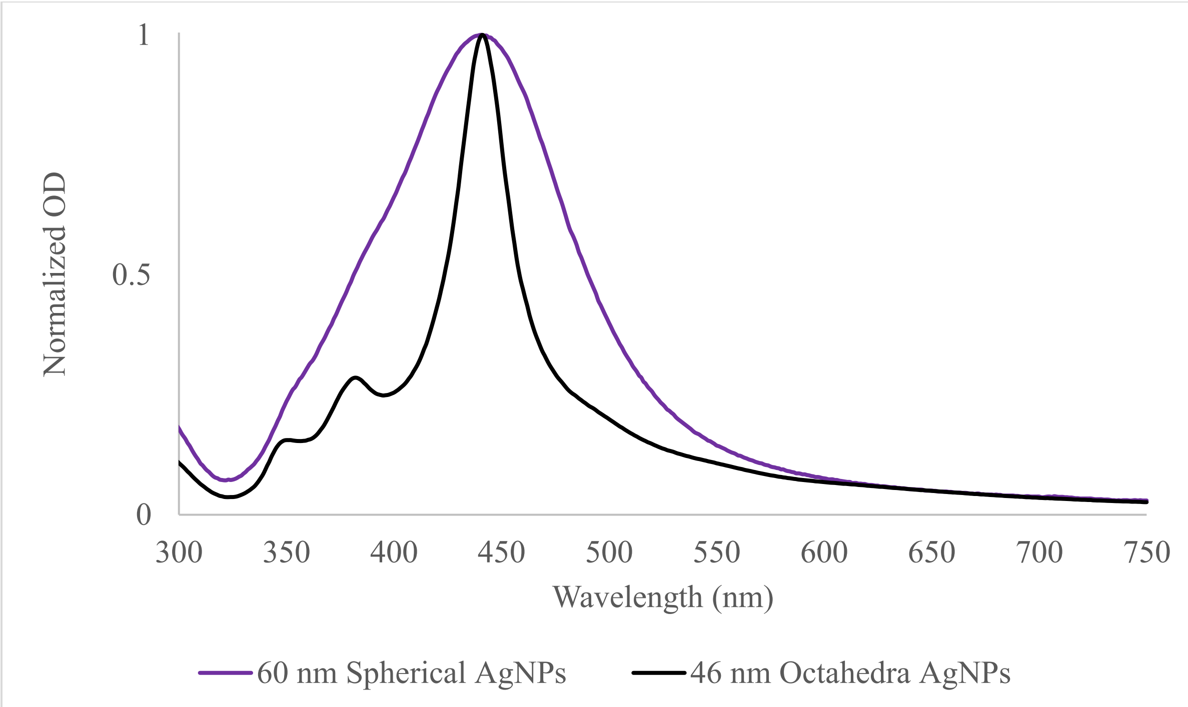

Figure 11. Direct comparison of the normalized OD spectras of commercial spherical AgNPs and octahedra AgNPs with comparable LSPR peaks.

Our synthesis protocol yields nanoparticles of greater uniformity of size and shape. In addition, our nanoparticles appear more symmetrical and possess sharper features compared to commercial AgNPs as seen in Figure 12. The combination of these factors allows for the attainment of LSPR peaks at more red-shifted wavelengths and narrow FWHM values. This maximizes the amount of harmful blue light wavelengths that can be filtered out, while allowing for transmission of beneficial blue light wavelengths.

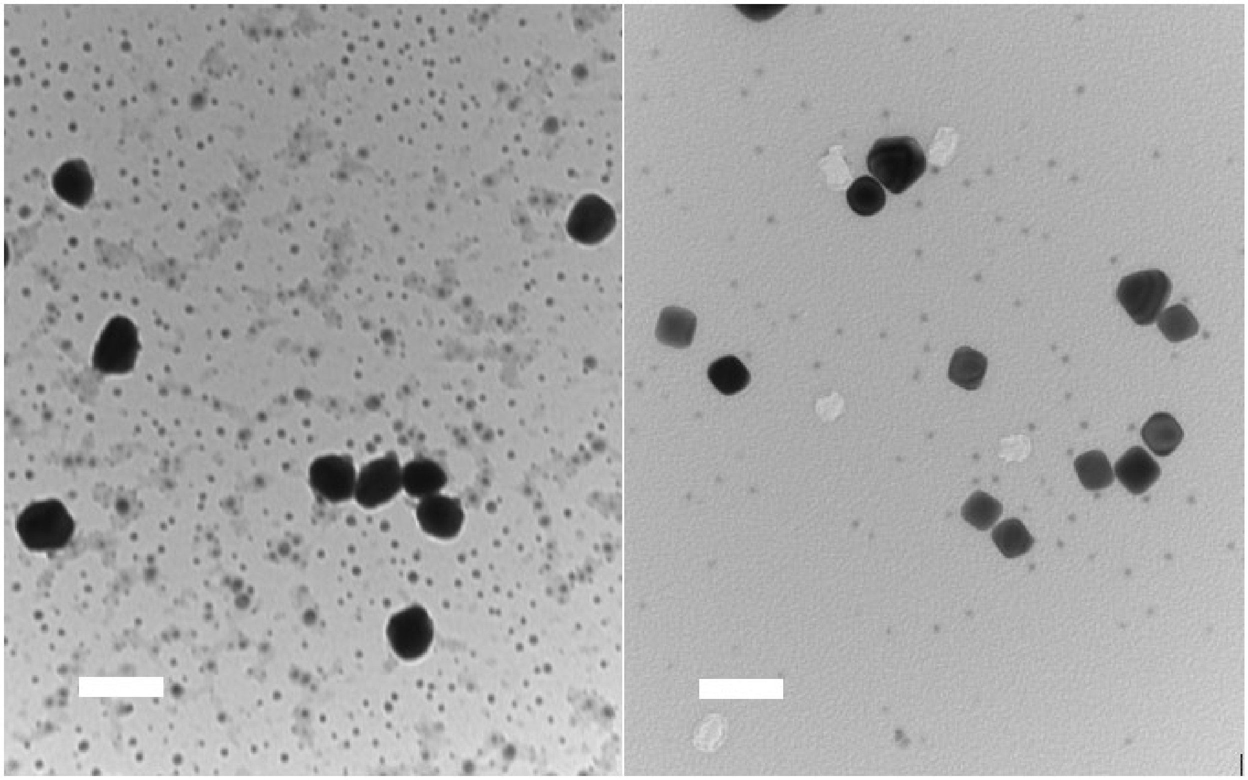

Figure 12. TEM images of commercial AgNPs (left) and octahedra AgNPs (right) synthesized using the optimized conditions of the polyol method. Scalebars represent 100 nm.

3.4. Conclusions

In conclusion, this chapter focused on tuning the polyol synthesis through controlling parameters that affect the growth kinetics and shape of the NPs. This is the first reported demonstration of using Cl^- ions to selectively synthesize cubic or octahedra AgNPs in a one-pot polyol synthesis. Under these optimized synthesis conditions, AgNPs with LSPRs > 440 nm and narrow FWHM values (<45 nm) can be produced. The LSPR can also be red-shifted over a range of ~40 nm (from 405 to 445 nm) without compromising the FWHM. The synthesis can be easily monitored over time and quenched once the LSPR is at the desired wavelength. In addition, the FWHM values of the LSPR peaks associated with these NPs are far superior to commercially available AgNPs. This work shows great promise for the utilization of AgNPs as selective blue light filters.

Chapter 4. Integration of NPs into contact lenses

4.1. Introduction

With over 71 million users worldwide, contact lenses are an attractive platform for incorporating blue light filters [11]. There are currently no commercially available contact lenses on the market offering both UV and blue light protection, although several patents have been issued [12, 13, 14, 15]. Most of these blue light filtering contact lens patents describe methods of incorporating blue light-absorbing molecules that are copolymerized with the polymer(s) used to manufacture the lenses. This is to eliminate potential leaching of blue-light absorbing molecules. The use of blue light absorbing dyes in contact lenses poses several limitations including low tunability of wavelengths that are absorbed, and their effect on the kinetics of polymerization (especially if a significant amount of the blue light absorbing agent is added to the monomer mixture). In addition, contact lenses are most commonly fabricated using cast molding in the industry, and this typically involves curing the polymers under UV (or HEV light) to form the lens. A longer cure time or increased light intensity may be required to circumvent for light that is absorbed by the HEV light absorbing agent during photocuring. The caveat is that increasing the curing time may affect the final properties of the lens [88].

The AgNPs prepared in Chapter 3 present a novel and promising approach to selective filtering of blue light wavelengths in contact lenses while overcoming some of the limitations of using blue light absorbing dyes. The high level of LSPR tunability shown in Chapter 3 allows for the development of custom blue light filters. This level of tunability is beneficial as it allows for the LSPR to be moved to wavelengths outside the peak emission of the photocuring lamps. It also allows for high transparency of blue light wavelengths that are beneficial to human health.

However, bare AgNPs are poorly suited for the harsh conditions required for selective light filtering in contact lenses. Without a protective coating, the optical properties of AgNPs may be compromised due to particle aggregation, etching, or reshaping [114]. Silica coating has gained increasing popularity as a tool to improve the stability of plasmonic nanoparticles and facilitate their integration into biomedical devices [115, 116]. In addition, silica coating has also been shown to inhibit the oxidative etching of silver and reduce its toxicity by preventing leakage of ions from the cores [123, 124].

For contact lens applications, encapsulating individual plasmonic AgNPs with thick silica shells has the potential to impart greater colloidal stability, protect the cores from the surrounding medium, attain a higher degree of control over the optical properties in harsh environments, and minimize/prevent leaching of Ag^+ ions. In addition, the protective silica layer around the plasmonic cores help stabilize the optical properties of the cores in the contact lens under autoclaving, and subsequent storage at room temperature.

In this chapter, the real-world utility of the nanoparticles developed in Chapter 3 is demonstrated. The following are presented herein:

(1) Successful integration of silica-coated AgNPs into etafilcon contact lenses using protocols that can be transferred to large-scale industry production.

(2) High transparency in the visible wavelengths and selective blue light filtering capabilities of AgNP integrated lenses.

(3) Comparative optical measurements of NP-integrated lenses after autoclaving and exposure to UV and natural sunlight.

(4) High optical stability of NP-integrated lenses over a 2-week storage period post-autoclaving, and UV exposure.

(5) Minimal leaching of nanoparticles and Ag^+ ions from the etafilcon lenses during storage.

4.2. Materials and methods

4.2.1. **Chemicals and materials**

Tetraethyl orthosilicate (TEOS, 99.999% trace metals basis), ammonia (28-30% NH_3 basis), poly(vinylpyrrolidone) (PVP, MW ≈ 55, 000), acetone, and anhydrous ethanol (EtOH, <0.003% H_2O) were purchased from Sigma-Aldrich. All chemicals were used as received. The silica coating of AgNPs were carried out in 20 mL glass scintillation vials, purchased from VWR. A filtration device was purchased from EMD Millipore to produce Millipore-grade water (>15 MΩ.cm).

All glassware was cleaned prior to use with 12 M NaOH for 1 hour followed by washing with copious amounts of DI water, and 3 washes of Millipore-grade water. Stir bars were cleaned with nitric acid for 10 minutes, followed by washing with copious amount of Millipore-grade water.

Contact lens molds, etafilcon monomer mixture and blue light emitting lamps (NARVA LT 40 W-K, peak emission ~420-430 nm) were received from Johnson and Johnson Vision Care. 20 mL glass scintillation vials and 8 mL autoclavable vials were purchased from VWR. Lenses were stored in 20 mL scintillation vials filled with 7 mL MDI.

4.2.2. **AgNPs**

Cubic AgNPs were prepared using the optimized polyol synthesis conditions described in section 3 (e.g. temperature set at 115 °C, 120 minute reaction duration). Octahedra AgNPs were also prepared at 115 °C, however the reaction duration was shortened to 105 minutes. A second octahedra AgNP sample (that was not silica coated) was prepared with slight variations in the synthesis to yield a more red-shifted LSPR peak. The reaction time was increased to 120 minutes and 7 ml of EG were added to the scintillation vial, instead of 5 ml.

The synthesis was quenched by immersing the scintillation vial in an ice bath. The final NP suspension was split into 3 mL portions, to which 50 mg of PVP were introduced. The NPs were precipitated with acetone and re-suspended in 3 mL EtOH, following centrifugation at 10000 RPM for 13 minutes.

4.2.3. **Coating of AgNPs**

The AgNPs were coated with silica following a modified Stober-like growth process. [140] A 10% TEOS solution (vol/vol %) was prepared in EtOH. 250 ul of ammonia and 100 ul of TEOS (10%) were introduced to the NP suspension in EtOH under magnetic stirring. The coating process continued over 12 hours, during which time the scintillation vial was capped, and aliquots were taken every few hours with a micropipette. Following the 12 hour silica coating, the NPs were washed with EtOH two times and collected via centrifugation at 10000 RPM for 13 minutes. Following 2 rounds of centrifugation, the NPs were re-suspended in EtOH and stored in the fridge (2 °C) until further use. All aliquots were diluted with MDI prior to TEM and UV-Vis analysis.

4.2.4. **Lens photocuring**

Silica-coated AgNPs (suspended in EtOH) were introduced into etafilcon monomer mixture at low volume concentrations (<10:140 vol/vol %). NPs were dispersed throughout the monomer mixture through vortexing. Six drops of the NP-monomer mixture were added to the back molds using a Pasteur pipette. The front molds were placed on top of the back molds (containing the monomer mixture). Molds were placed underneath the blue light emitting lamps for 20 minutes to photo-cure the monomer mixtures. After photocuring, the front molds were pried off the back molds and the back molds (containing the etafilcon lens) were placed in a hot DI water bath (set at 70 °C) to separate the NP-integrated contact lenses from the molds.

4.2.5. **UV exposure**

The stability of the synthesized NP-integrated etafilcon lenses was tested under an array of UVA fluorescent bulbs (Philips F20T12/BL., Amsterdam, Netherlands, peak emission ~350 nm) in an enclosed environment. The lenses were contained in transparent Gladwrap-sealed 20 mL scintillation vials filled with 7 mL of MDI. The UV intensity was measured to be ~33.96 W/m^2 with a UVA/B light meter (Sper Scientific, Scottsdale, AZ, USA, NIST certified calibration) which is slightly lower than the UV content of the solar spectrum (ASTM G173-03 global tilt) [141]. Cumulative UV exposure was adjusted such that lenses would receive the equivalent of 1, 3.5 or 7 days of solar UV exposure with the assumption that UV contributes to 4.72% of cumulative insolation [142].

4.2.6. **Solar exposure**

The stability of the prepared NP-integrated etafilcon lenses was tested under natural sunlight exposure in Waterloo, Ontario. The lenses were placed in clear 20 mL scintillation vials filled with MDI and left outdoors during peak sunlight hours (10:00 AM to 4:15 PM). Weather data was obtained from the University of Waterloo Weather Station [143]. See Appendix E for solar irradiation data.

4.2.7. **Autoclaving**

NP-integrated etafilcon lenses were autoclaved for 20 minutes at 121°C and 1.1 bar. Lenses were placed in loosely sealed 8 mL autoclavable glass, filled with 6 mL of MDI.

4.2.8. **Characterization**

TEM

The size and shape of the nanoparticles were analyzed with a Philips CM-10 transmission electron microscope (TEM).

Optical Measurements

The OD spectra of the contact lenses were measured using a spectrophotometer (BioTek Epoch, Take3 Plate).

ICP Sample Preparation of NP-Integrated Contact Lenses

5 mL of the storage solution was diluted with 0.2 mL of concentrated nitric acid (70%) and left undisturbed over 1 day to acid-digest any nanoparticles that may be present in solution. After the initial acid digestion, 4.8 mL of dilute nitric acid (0.7%) was introduced and the solution was left undisturbed for at least 24 hours.

ICP Sample Preparation of Silica-coated AgNP

Silica-coated AgNPs were acid digested in a similar manner to the storage solution used to hydrate the contact lenses.

ICP Analysis

ICP-(OES) analysis for Ag^+ ions were carried out using the model ProdigyPlus (Teledyne Leeman Labs). The detection range of this instrument was 15 ppb to 80 ppm and the lower limit of detection (LLOD) was found to be 15 ppb for Ag^+ detection in MDI. Calibration standards containing 0, 9.6, 16, 32 and 80 ppm Ag as well as an internal standard of 10 ppm yttrium were used. Data was collected using Salsa software.

4.3. Results and discussion

4.3.1. **Silica coating – Preparing colloidally stable plasmonic NP-based filters**

Both cubic and octahedra NPs were successfully coated with silica. On average, the silica coating red-shifts the LSPR by ~10 nm with minimal changes in the FWHM of the LSPR peak.

This red-shifting is attributed to silica having a higher refractive index than water [114]. In addition, the characteristic plasmonic peaks/shoulders associated with cubic and octahedra structures are retained post-silica coating as seen in Figure 13. High transparency in the visible wavelengths is also retained, revealing silica coating is an effective means to further tune the LSPR peak, without hindering the FWHM.

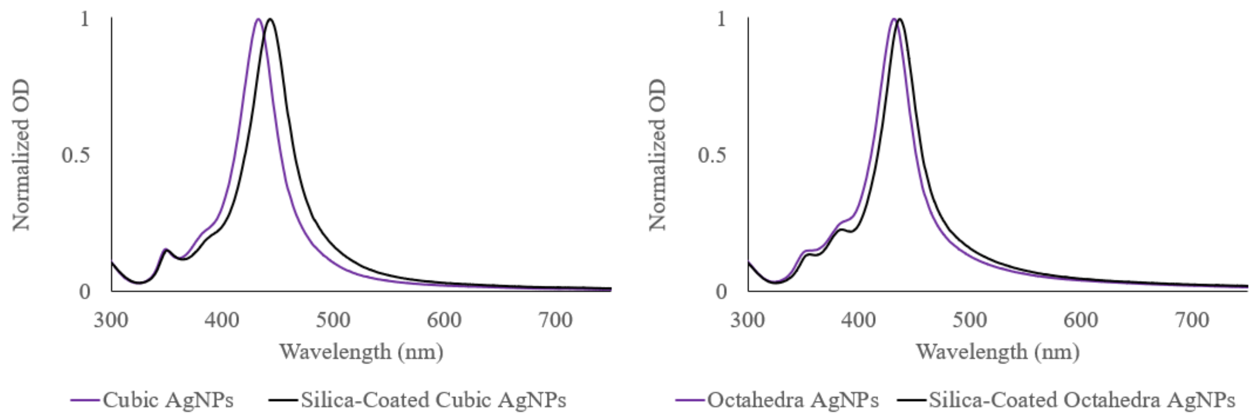

Figure 13. Normalized OD spectras of cubic AgNPs (left) and octahedra AgNPs (right) before and after silica coating.

TEM analysis revealed the coating process led to the deposition of a thick, uniform shell around individual plasmonic nanoparticles, as seen in Appendix C. The sharp features of the Ag cores were also retained throughout the entirety of the coating and washing process. The successful deposition of thick silica layers is due to finite control over the relative concentrations of ammonia, TEOS, and AgNPs, as well as the coordinating effect of PVP. Fine control over the relative ratios of these components are necessary to ensure that heterogenous nucleation of silica were favourable over homogenous nucleation of silica nanoparticles [114]. The presence of PVP on the surface of the AgNPs also aids in the early stages of silica deposition. Apart from improving the colloidal stability of the NPs, PVP also makes the AgNPs vitreophillic through its high affinity for silica [140]. The high affinity arises from electrostatic interactions and hydrogen bonding between the positively charged groups of PVP and negatively charged silica [144].

The stability of the silica-coated AgNPs were monitored at room temperature over a 4-week period. The LSPR tends to blue-shift by a few nanometers (6-7 nm) over time, however there are minimal changes in the FWHM of the LSPR peak and OD values of the LSPR, as seen in Table 9.

Table 9. Optical stability of silica-coated AgNPs stored at room temperature. Top, middle and bottom values in each cell correspond to the LSPR, FWHM and OD respectively.

Silica-coated Sample	Initial	1 Week	2 Week	4 Week
Octahedra	437 40 1.143	431 37 1.147	431 38 1.086	430 37 1.109
Cubic	442 43 1.968	438 42 1.916	436 42 1.916	436 42 1.879

The slight blue-shifting in LSPR peak may be due to surface rearrangement and rounding out of the corners as seen in Figure 14. The TEM images in Figure 14 reveal the features of the Ag cores to be sharper prior to room temperature storage. The silica shell appears to be stable throughout this storage period. The high stability of this protective shell layer is essential to preserve the optical properties of the plasmonic cores and to prevent irreversible aggregation over time.

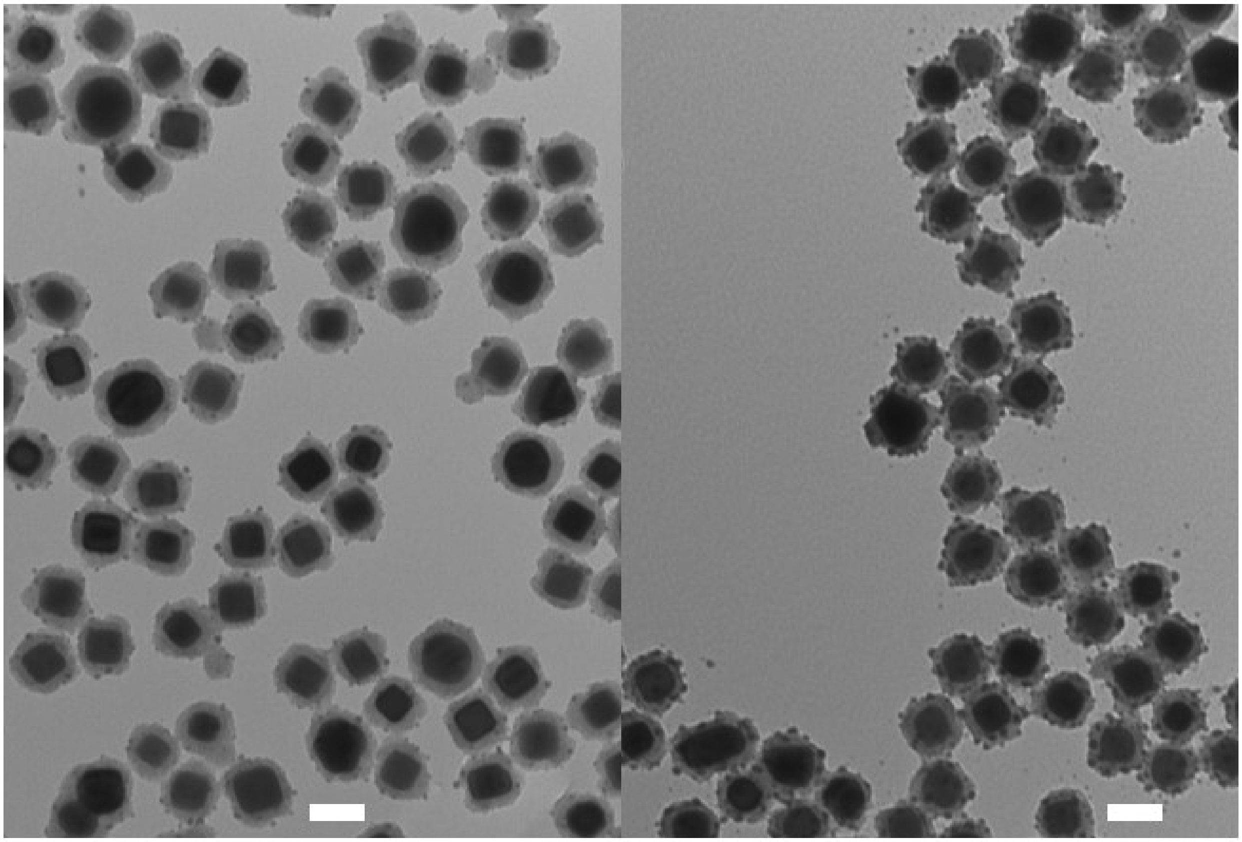

Figure 14. TEM images of silica-coated cubic AgNPs stored in the fridge (left) and after 2 weeks of storage at room temperature (right). Scalebars represent 50 nm.

4.3.2. **Integration of NPs into contact lenses**

Silica-coated cubic and octahedra AgNPs were successfully integrated into etafilcon hydrogel lenses through photocuring. The fabricated lenses show good mechanical and optical properties. As seen in Figure 15, the fabricated lenses are transparent and devoid of any visible defects. The high transparency of the lenses suggests that the nanoparticles are well dispersed and non-aggregated in the hydrogel lens. The yellow tint is inevitable given the blue light filtering properties imparted on the lenses by the plasmonic nanoparticles. Apart from the yellow tint, the NP-integrated lenses appear comparable to commercial etafilcon contact lenses. Since the NPs were introduced into the monomer mixtures at low volume/volume ratios (<10:140), the relative concentrations of the various components in the monomer mixture (e.g. initiator, monomer, UV blocking agent, etc.) were minimally affected. As a result, photo-initiated polymerization proceeded smoothly, and a 20-minute curing period proved to be effective in preparing mechanically stable and transparent blue light filtering contact lenses.

Figure 15. NP-integrated lenses show high transparency and are devoid of visible defects.

Three key findings were made upon measuring the optical properties of the NP-integrated contact lenses:

(1) The LSPR of silica-coated AgNPs blue-shifts by a few nanometers.

(2) The LSPR of uncoated AgNPs red-shifts.

(3) The LSPR peak generated by silica-coated AgNPs shows minimal broadening post-integration.

The red-shifting of the LSPR peak (as seen in Table 10) generated by bare AgNPs is unsurprising given the nanoparticles have been transferred into a matrix with a higher refractive index and may be in closer proximity to one another. The silica-coated AgNPs do not show a red-shift in LSPR post-integration and this may be attributed to the role of the protective silica layer around the plasmonic cores. Even though the NPs have been transferred to a matrix of higher refractive index than water, silica remains the immediate surrounding layer around the plasmonic cores. Thus, the plasmonic cores should not be significantly affected by any changes in the refractive index surrounding the silica layer. In addition, the thick layer of silica surrounding the plasmonic cores serves as an effective spacer layer between adjacent cores. This prevents their electric fields from being coupled which would lead to a red-shift in LSPR and increase in FWHM. There is a slight blue shift in the LSPR peak post-integration of silica-coated AgNPs which may be due to a combination of photo-oxidation, surface rearrangement, and rounding out of the sharp features of the nanoparticles.

Table 10. Optical properties of NPs and NP-integrated lenses.

Sample	Pre-Lens Integration		Post Lens Integration		
	LSPR	FWHM	Lens No	LSPR	FWHM
Octahedra AgNPs	436-437	39	1	443-445	44
			2	443-445	46
			3	444-445	45
			4	443-444	42
Silica-Coated Octahedra AgNPs	437	40	1	436	44
			2	434-436	48
			3	433-434	47
			4	431-432	45
			5	429-431	41
Silica Coated Cubic AgNPs	441	43	1	433-434	47
			2	435	47
			3	431-434	46
			4	429-430	46
			5	430-432	46

Apart from the slight blue-shift in the LSPR peak, the optical properties of the NP-integrated lenses are exceptional, as seen in Figure 16. The lenses possess both UV and high energy blue-light filtering capabilities while being highly transparent in the visible regions.

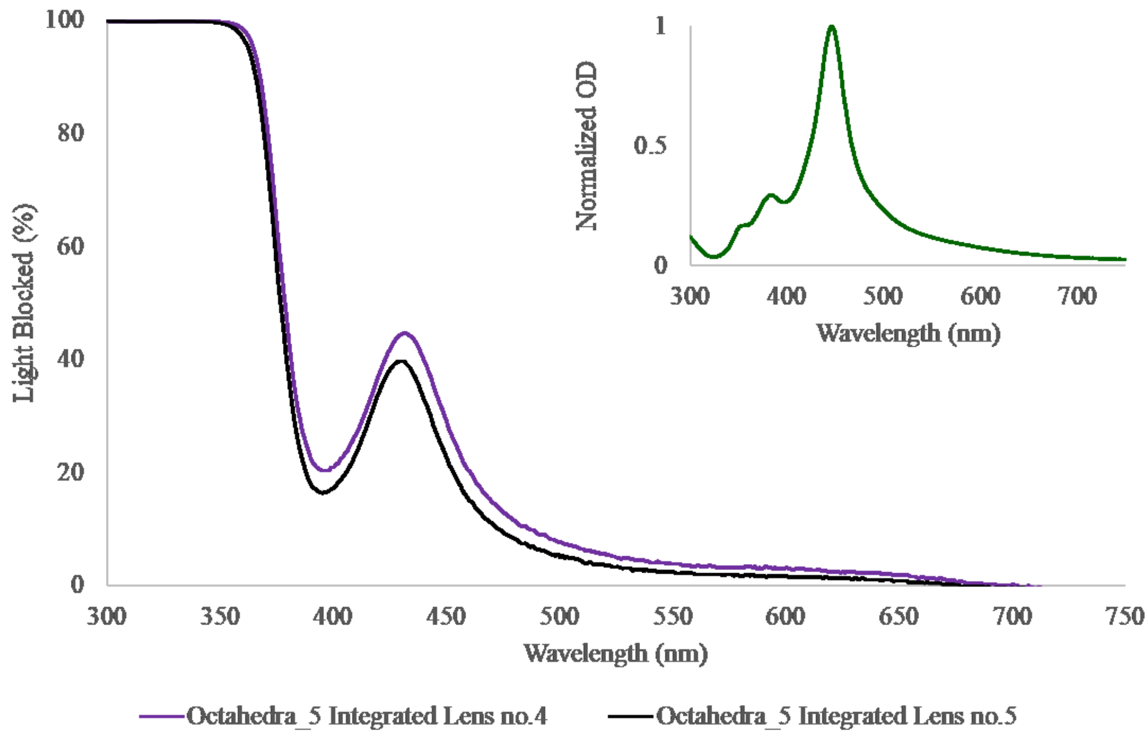

Figure 16. Light blockage spectra of lens no.4 and 5 of silica-coated octahedra AgNP-integrated etafilcon lenses. Inset is the normalized OD spectra of silica-coated octahedra AgNPs (in water) prior to integration.

4.3.3. **Stability under UV exposure**

The optical properties of silica-coated AgNP integrated lenses were monitored after exposure to UVA light in an enclosed setting. The lenses received doses equivalent to 1, 3.5 and 7 days of UV exposure from natural sunlight (during peak hours). There is a slight blue-shift in the LSPR after “1 day” of UV exposure as seen in Table 11. The LSPR appears to stabilize after this initial blue shift, as further UV exposure has minimal effects on the LSPR. No significant changes in the FWHM were observed. The initial blue shift may be due to the formation of an oxide layer around the plasmonic cores due to photo-oxidation. The presence of this layer comes at the expense of rounding out of corners and sharp features of the plasmonic cores [145]. This oxide layer may then act as a protective layer, preventing further oxidation of the Ag cores. As a result, further UV exposure has no noticeable change on the optical properties of the NP-integrated lenses.

Table 11. The effects of UV exposure on the optical properties of NP-integrated lenses. Control lenses were not exposed to UV light.

Control		1 Day		3.5 Days		1 Week	
LSPR	FWHM	LSPR	FWHM	LSPR	FWHM	LSPR	FWHM
436	44	428	42	428-430	45	428	41
434-436	48	428	46	429-430	45	427-428	43
433-434	47	428	44	430-432	41	427-429	42
431-432	45	429-430	41	427-429	42	428-429	42
429-431	41	428-429	43	429-430	41	426-428	44

The light blockage profile of lenses exposed to UV exposure appear comparable to non-UV exposed lenses. The inset in Figure 17 reveals no noticeable difference in the aesthetics of the lenses after "1 week" of UV exposure.

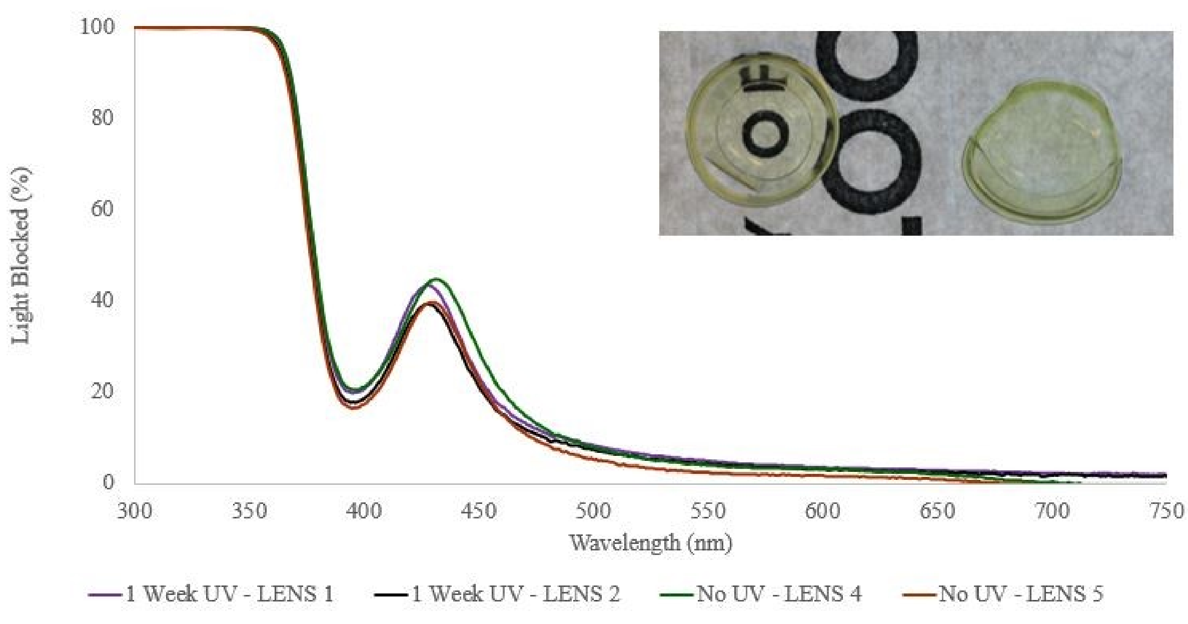

Figure 17. Light blockage profile of control NP-integrated lenses and lenses that received the equivalent of "1 week" of UV dose. The inset depicts NP-integrated lenses that received 1 week of UV exposure (left) control NP-integrated lenses (right).

4.3.4. **Stability under solar exposure**

The silica-coated AgNP-integrated lenses were also tested under natural sunlight conditions. Once again, a slight blue-shift in the LSPR peak was observed due to photo-oxidation. Aside from lens no.1, there were no noticeable increases in the FWHM of the LSPR peak.

Table 12. The effects of natural sunlight exposure on the optical properties of NP-integrated contact lenses.

	Initial		Solar Exposure	
No	Peak	FWHM	Peak	FWHM
1	436	44	429-431	56
2	434-436	48	433-434	45
3	435-436	43	433	43
4	436	54	431	43

4.3.5. **Stability under autoclaving**

NP-integrated lenses were autoclaved to assess their compatibility with industrial sterilization processes. The LSPR peak blue-shifts after autoclaving as seen in Table 13. The rate of oxidation may be catalysed at the increased pressure and temperature conditions of the autoclave. In addition, the gas permeability of the lenses may be elevated under autoclaving, which results in the entrapped nanoparticles being exposed to a higher dose of oxidizing agents.

Table 13. The effects of autoclaving on the optical properties of NP-integrated contact lenses.

	Control Lenses			Autoclaved Lenses	
No	Peak	FWHM	No	Peak	FWHM
1	436	44	1	424-425	42
2	434-436	48	2	425	44
3	433-434	47	3	423	46
4	431-432	45	4	417-419	45
5	429-431	41	5	426-428	45

Apart from blue-shifting of the LSPR peak, there were no noticeable abnormalities in the light blockage spectra of the autoclaved lenses (as seen in Figure 18).

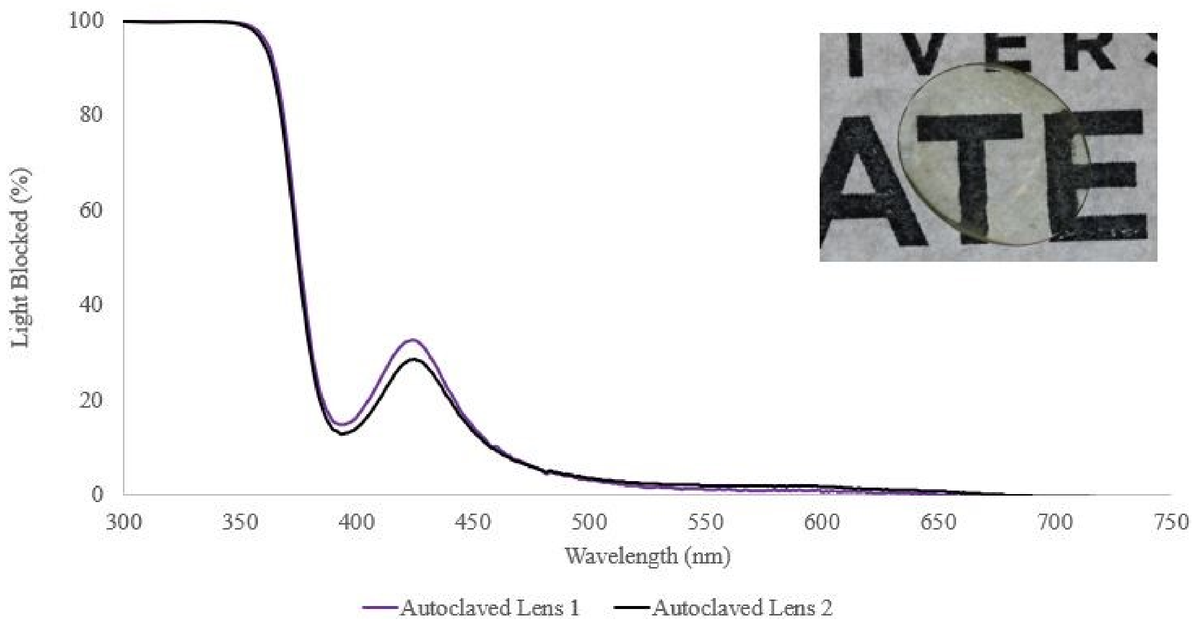

Figure 18. Light blockage spectra of autoclaved lenses. Inset depicts AgNP-integrated lens post-autoclaving.

4.3.6. **Room temperature storage**

The stability of the lenses was studied over time at room temperature. Table 14 compares the stability of UV exposed lenses to the control lenses (which didn't receive UV exposure). There were no significant changes in the LSPR peak and FWHM after 2 weeks of storage.

Table 14. Optical stability of UV-exposed lenses during storage.

Control Lenses			UV-Exposed Lenses				
			After 1 Week UV Exposure			2 Weeks Storage Post-UV	
No	Peak	FWHM	No	Peak	FWHM	Peak	FWHM
1	436	44	1	428	41	427-428	39
2	434-436	48	2	427-428	43	428	41
3	433-434	47	3	427-429	42	428	40
4	431-432	45	4	428-429	42	427	44
5	429-431	41	5	426-428	44	425-427	41

The optical stability of autoclaved lenses was also investigated to get a sense of the shelf life of sterilized NP-integrated lenses. As seen in Table 15, there is minimal blue-shifting and broadening of the LSPR post-storage.

Table 15. Optical stability of autoclaved lenses during storage.

Control Lenses			Autoclaved Lenses				
				After Autoclaving		2 Weeks Storage	
No	Peak	FWHM	No	Peak	FWHM	Peak	FWHM
1	436	44	1	424-425	42	421-422	47-48
2	434-436	48	2	425	44	425	45
3	433-434	47	3	423	46	421-424	47
4	431-432	45	4	417-419	45	416-418	48*
5	429-431	41	5	426-428	45	426	49

* See Appendix F.

4.3.7. **Quantitation of leaching from NP-integrated lenses using ICP**

ICP analysis was conducted to determine the combined extent of Ag^+ ion and nanoparticle leaching from the NP-integrated lenses. ICP analysis was conducted on the MDI storage solution that the lenses were stored in (for >3 weeks) after fabrication (for control lenses), during and after UV exposure (for UV-exposed lenses) and post-autoclaving (for autoclaved lenses). The total mass of silver initially integrated into the contact lenses is estimated to be ~12.401 ug (Appendix G). Minimal leaching occurred over the storage period, and in some cases the amount of leaching was less than the LLOD of the system (<210 ng or <1.7%). The results are summarized in Table 16.

Table 16. Leaching of silver from control, autoclaved and UV exposed NP-integrated lenses determined by ICP.

	No	Total Mass of Leached Silver (ng)	Percentage of Silver Leached from Lens (%)
Control	1	<210.0	<1.7
	2	<210.0	<1.7
	3	380.4	3.1
	4	<210.0	<1.7
	5	<210.0	<1.7
Autoclaved	1	382.8	3.1
	2	428.4	3.5
	3	526.8	4.2
	4	357.6	2.9
	5	381.6	3.1
7 Days of UV Exposure	1	264.6	2.1
	2	546.0	4.4
	3	429.8	3.5
	4	383.6	3.1
	5	203.0	1.6

4.4. Conclusions

In summary, silica-coated AgNPs were successfully integrated into etafilcon contact lenses to impart selective blue light filtering capabilities while retaining high transparency in the visible wavelengths. The NP-integrated lenses show good mechanical properties (e.g. lenses do not tear easily) and are devoid of any visible deformations. In addition, the NP-integrated lenses show good stability under autoclaving, UV, and natural sunlight exposure. Furthermore, ICP analysis revealed very low percentages of leached nanomaterials and/or ions from the lenses during storage.

Chapter 5. Conclusions & Future Work

5.1. Conclusions

The goal of this thesis was to address a critical market void in blue light blocking eyewear by synthesizing plasmonic silica-coated AgNPs and integrating them into commercial etafilcon contact lenses. A thorough literature review was conducted to determine the impact of various blue light wavelengths on ocular and non-ocular health, the current pitfalls in developing notch filters in eyewear, and the selective light filtering capabilities of plasmonic nanoparticles. Based off this, it was determined that silica-coated AgNPs would make for an excellent candidate to block selective wavelengths of blue light in contact lenses. The morphology of the plasmonic Ag cores could be tuned to adjust their LSPR peak throughout the blue light wavelengths, while the deposited silica shell could impart greater colloidal and chemical stability, improve the biocompatibility of the plasmonic materials (by preventing/minimizing leaching of Ag^+ ions), and facilitate integration into contact lenses.

The first phase of this research focused on investigating the polyol process to develop a tunable synthesis process that allows for the production of notch silver nanoparticle-based filters with customizable optical properties. Through careful control over the growth kinetics and shape-directing agents, a synthesis protocol was developed that allows the LSPR peaks of the AgNPs to be tuned between 400 – 450 nm with FWHM values of less than 45 nm.

Phase 2 focused on depositing a thick, uniform layer of silica around individual AgNPs to serve as a protective layer. The silica-coated NP were shown to be colloidally and optically stable under storage at room temperature and for months in the fridge. The silica coating also proved to be a tool that could be exploited to further red-shift the LSPR of the plasmonic Ag cores, without compromising the FWHM.

Lastly, phase 3 focused on integrating silica-coated AgNPs into etafilcon hydrogels and demonstrating stability during sterilization processes (autoclaving), UV and sunlight exposure, and room temperature storage. Silica-coated AgNPs were successfully integrated into etafilcon contact lenses using methods that can be transferred to large-scale industry production. The silica-coated AgNPs imparted notch blue light filtering capabilities on commercial etafilcon contact lenses while retaining high transparency in the visible wavelengths. In addition, the NP-integrated lenses showed comparative optical measurements after autoclaving and exposure to UV and natural sunlight. High optical stability of the NP-integrated lenses was demonstrated over a 2-week storage period post-autoclaving and UV exposure, as well as minimal leaching of silver from the etafilcon lenses.

5.2. Future Work

The research objectives highlighted in section 1.2 were met through this research project, and paved the way for future studies. The next steps are to further tune and improve upon the optical properties of the silica-coated AgNPs and to continue assessing the stability, mechanical, and optical properties of NP-integrated lenses.

The polyol process can be further investigated to determine whether the nanoparticle synthesis can be tuned to generate LSPR peaks at even more red-shifted wavelengths (>450 nm) while retaining narrow FWHM values (<45 nm).

Further testing of NP-integrated lenses is required to determine their utility in commercial applications. The shelf-life of the NP-integrated lenses should be investigated along with their compatibility with commercial packing solutions. A series of studies should also be conducted to estimate the lifetime and optical stability of the NP-integrated lenses during consumer wear. Optical measurements and ICP analysis can be routinely conducted as the NP-integrated lenses are exposed to various external conditions, such as natural and artificial lighting, changes in temperature, and mechanical agitation to simulate blinking of the eyelids, while being immersed in simulated tear fluid. Preliminary *in vivo* studies should also be carried out to determine the mechanical stability and biocompatibility of the synthesized lenses.

References

[1] F. Behar-Cohen, C. Martinsons, F. Vienot, G. Zissis, A. Barlier-Salsi, J. P. Cesarini, O. Enouf, M. Garcia, S. Picaud and D. Attia, "Light-emitting diodes (LED) for domestic lighting: Any risks for the eye?," *Progress in Retinal and Eye Research,* vol. 30, no. 4, pp. 239-257, 2011.

[2] D.-C. Chen, K.-L. Huang, S.-L. Lee and J.-T. Wang, "Blue Light Blocking Lenses Measuring Device," *Procedia Engineering,* vol. 140, pp. 17-29, 2016.

[3] K. N. Paul, T. B. Saafir and G. Tosini, "The role of retinal photoreceptors in the regulation of circadian rhythms," *Reviews in Endocrine and Metabolic Disorders,* vol. 10, no. 4, pp. 271-278, 2009.

[4] K. Smick, T. Villette, M. E. Boulton, G. C. Brainard, W. Jones, P. Karpecki, R. Melton, R. Thomas, D. H. Sliney and D. Shechtman, "Blue Light Hazard: New Knowledge, New Approaches to Maintaining Ocular Health," Essilor of America Inc, New York City, 2014.

[5] W. T. Ham, H. A. Mueller, J. J. Ruffolo and A. M. Clarke, "Sensitivity of the retina to radiation damage as a function of wavelength," *Photochemistry and Photobiology,* vol. 29, no. 4, pp. 735-743, 1979.

[6] W. T. Ham, H. A. Mueller and D. H. Sliney, "Retinal sensitivity to damage from short wavelength light," *Nature,* vol. 11, pp. 153-155, 1976.

[7] A. Main, I. Vlachonikolis and A. Dowson, "The wavelength of light causing photophobia in migraine and tension-type headache between attacks," *Headache,* vol. 40, no. 3, pp. 194-199, 2000.

[8] J. M. Stringham, K. Fuld and A. J. Wenzel, "Action spectrum for photophobia," *Journal of the Optical Society of America A,* vol. 20, no. 10, pp. 1852-1858, 2003.

[9] P. A. Good, R. H. Taylor and M. J. Mortimer, "The use of tinted glasses in childhood migraine," *Headache,* vol. 31, no. 8, pp. 533-536, 1991.

[10] Y. Z. Rosenblum , P. P. Zak, M. A. Ostrovsky and et al, "Spectral filters in low-vision correction," *Ophthalmic & Physiologic Optics,* vol. 20, no. 4, pp. 335-341, 2000.

[11] "The Danger of Using Tap Water with Contact Lenses," United States Environmental Protetion Agency, 18 January 2018. [Online]. Available: https://www.epa.gov/dwstandardsregulations/danger-using-tap-water-contact-lenses. [Accessed 13 June 2018].

[12] J. W. Haywood, L. G. Jones and J. W. Dukes, "CONTACT LENSES WITH LIGHT BLOCKING RINGS". US Patent US007364291B2, 29 April 2008.

[13] K. Mentak, "ULTRA VIOLET, VIOLET, AND BLUE LIGHT FILTERING POLYMERS FOR OPHTHALMIC APPLICATIONS". US Patent US007842367B2, 30 November 2010.

[14] M. D. Christ, "OPHTHALMIC LENS HAVING A YELLOW DYE LIGHT BLOCKING COMPONENT". US Patent US008394906B2, 12 Mar 2013.

[15] H. Bothe, Y. Qiu and P. Hagmann, "METHOD FOR MAKING UV-ABSORBING OPHTHALMIC LENSES". US Patent US20130095235A1, 18 April 2013.

[16] U. Kreibig and M. Vollmer, Optical Properties of Metal Clusters, New York: Springer, 1995.

[17] M. A. El-Sayed, "Some interesting properties of metals confined in time and nanometer space of different shapes," *Accounts of Chemical Research,* vol. 34, no. 4, pp. 257-264, 2001.

[18] U. Kreibig and L. Genzel, "Optical absorption of small metallic particles," *Surface Science,* vol. 156, pp. 678-700, 1985.

[19] R. Sperling and W. Parak, “Surface modification, functionalization and bioconjugation of colloidal inorganic nanoparticles,” *Philosophical Transactions of the Royal Society A,* vol. 368, pp. 1333-1383, 2010.

[20] A. Delgado-Bonal and J. Martin-Torres, “Human vision is determined based on information theory,” *Scientific Reports,* vol. 6, 2016.

[21] Z. Yang and D. Purves, “A statistical explanation of visual space,” *Nature Neuroscience,* vol. 6, no. 6, pp. 632-640, 2013.

[22] D. H. Sliney, “How Light Reaches the Eye and Its Components,” *International Journal of Toxicology ,* vol. 21, no. 6, pp. 501-509, 2002.

[23] E. A. Boettner and J. R. Wolter, “Transmission of the ocular media,” *Investigative Ophtalmology & Visual Science,* vol. 1, no. 6, pp. 776-783, 1962.

[24] I. M. Pepe, “Rhodopsin and phototransduction,” *Journal of Photochemistry and Photobiology B,* vol. 48, pp. 1-10, 1999.

[25] R. P. Najjar, C. Chiquet, P. Teikari, P.-L. Cornut, B. Claustrat, P. Denis, H. M. Cooper and C. Gronfier, “Aging of Non-Visual Spectral Sensitivity to Light in Humans: Compensatory Mechanisms?,” *PLoS One,* vol. 9, no. 1, 2014.

[26] D. M. Berson, “Phototransduction in ganglion-cell photoreceptors,” *Pfluggers Archiv: European Journal of Physiology,* vol. 454, pp. 849-855, 2007.

[27] P. D. Gamlin, D. H. McDougal, J. Pokorny, V. C. Smith, K.-W. Yau and D. M. Dacey, “Human and Macaque Pupil Responses Driven by Melanopsin-Containing Retinal Ganglion Cells,” *Vision Research,* vol. 47, no. 7, pp. 946-954, 2007.

[28] R. Klein, B. Klein and K. Linton, “Prevalence of age-related maculopathy. The Beaver Dam Eye Study.,” *Ophthalmology,* vol. 99, no. 6, pp. 933-943, 1992.

[29] N. Congdon, B. O'Colmain, C. Klaver, R. Klein, B. Munoz, D. Friedman, J. Kempen, H. Taylor and P. Mitchell, “Causes and prevalence of visual impairment among adults in the United States,” *Archives of Ophthalmology,* vol. 122, no. 4, pp. 477-485, 2004.

[30] M. Rozanowska and T. Sarna, “Light-induced damage to the retina: role of rhodopsin chromophore revisited,” *Photochemical Photobiology,* vol. 81, no. 6, pp. 1305-1330, 2005.

[31] J. Sparrow and M. Boulton, “RPE lipofuscin and its role in retinal pathobiology,” *Experimental Eye Research,* vol. 80, no. 5, pp. 595-606, 2005.

[32] J. Sparrow, J. Zhou, S. Ben-Shabat, H. Vollmer, Y. Itagaki and K. Nakanishi, “Involvement of oxidative mechanisms in blue-light-induced damage to A2E-laden RPE,” *Investigative Ophthalmology & Visual Science,* vol. 43, no. 4, pp. 1222-1227, 2002.

[33] S. Finnemann, L. Leung and E. Rodriguez-Boulan, “The lipofuscin component A2E selectively inhibits phagolysosomal degradation of photoreceptor phospholipid by the retinal pigment epithelium,” *Proceedings of the National Academy of Sciences of the United States of America,* vol. 99, no. 6, pp. 3842-3847, 2002.

[34] S. Kaya, G. Weigert, B. Pemp, S. Sacu, R. Werkmeister and et al, “Comparison of macular pigment in patients with age-related macular degeneration and healthy control subjects – a study using spectral fundus reflectance,” *Acta Ophthalmology,* vol. 90, no. 5, pp. 399-403, 2012.

[35] R. Raman, R. Rajan, S. Biswas, K. Vaitheeswaran and T. Sharma, “Macular pigment optical density in a South Indian population,” *Investigative Ophthalmology & Visual Science,* vol. 52, no. 11, pp. 7910-7916, 2011.

[36] W. Gellermann, I. Ermakov, M. Ermakova, R. McClane, D. Zhao and P. Bernstein, “In vivo resonant Raman measurement of macular carotenoid pigments in the young and the aging human retina,”

Journal of the Optical Society of America. A, Optics, image science, and vision, vol. 19, no. 6, pp. 1172-1186, 2002.

[37] E. Arnault, C. Barrau, C. Nanteau and et al, "Phototoxic Action Spectrum on a Retinal Pigment Epithelium Model of Age-Related Macular Degeneration Exposed to Sunlight Normalized Conditions," *PLoS ONE,* vol. 8, no. 8, 2013.

[38] Y. J. Johnson, E. Shang, F. Shang and et al, "Measurement of Macular Pigment Optical Density in a Healthy Chinese Population Sample," *Investigative Ophtalmology & Visual Science,* vol. 53, no. 4, pp. 2106-2111, 2012.

[39] Macular Photocoagulation Study Group, "Argon laser photocoagulation for neovascular maculopathy. Three-year results from randomized clinical trials. Macular Photocoagulation Study Group.," *Archives of Ophthalmology,* vol. 104, no. 5, pp. 694-701, 1986.

[40] Macular Photocoagulation Study Group, "Argon laser photocoagulation for senile macular degeneration. Results of a randomized clinical trial," *Archives of Ophthalmology,* vol. 100, pp. 912-918, 1982.

[41] L. S. Lim, P. Mitchell, J. M. Seddon, F. G. Holz and T. Y. Wong, "Age-related macular degeneration," *The Lancet,* vol. 379, no. 9827, pp. 1728-1738, 2012.

[42] S. Daan and J. Aschoff, "Circadian Contributions to Survival," *Vertebrate Circadian Systems ,* pp. 305-321, 1982.

[43] C. S. Pittendrigh, "Temporal organization: reflections of a Darwinian clock-watcher," *Annual Review of Physiology ,* vol. 55, pp. 16-54, 1993.

[44] R. J. Lucas, S. Hattar, M. Takao, D. M. Berson, R. G. Foster and K. W. Yau, "Diminished pupillary light reflex at high irradiances in melanopsin-knockout mice," *Science,* vol. 299, no. 5604, pp. 245-247, 2003.

[45] G. C. Brainard, J. P. Hanifin, J. M. Greeson, B. Byrne, G. Glickman , E. Gerner and M. D. Rollag, "Action spectrum for melatonin regulation in humans: evidence for a novel circadian photoreceptor," *The Journal of Neuroscience,* vol. 21, no. 16, pp. 6405-6412, 2001.

[46] D. J. Dijk and C. Cajochen, "Melatonin and the circadian regulation of sleep initiation, consolidation, structure, and the sleep EEG," *Journal of Biological Rhythms ,* vol. 12, no. 6, pp. 627-635, 1997.

[47] G. Glickman, B. Byrne, C. Pineda, W. W. Hauck and G. C. Brainard, "Light therapy for seasonal affective disorder with blue narrow-band light-emitting diodes (LEDs)," *Biological Psychiatry,* vol. 59, no. 6, pp. 502-507, 2006.

[48] S. W. Lockley and J. J. Gooley, "Circadian photoreception: spotlight on the brain," *Current Biology,* vol. 16, no. 18, pp. R795-7, 2006.

[49] K. A. Roecklein, K. J. Rohan, W. C. Duncan, M. D. Rollag, N. E. Rosenthal, R. H. Lipsky and I. Provencio, "A missense variant (P10L) of the melanopsin (OPN4) gene in seasonal affective disorder," *Journal of Affective Disorders,* vol. 114, no. 1-3, pp. 279-285, 2009.

[50] H. R. Colten and B. M. Altevogt , Sleep Disorders and Sleep Deprivation, National Academies Press, 2006.

[51] L. S. Mure, P. L. Cornut, C. Rieux and et al, "Melanopsin bistability: a fly eye's technology in the human retina," *PLoS ONE,* vol. 4, no. 6, p. e5991, 2009.

[52] V. Francoise, S. Bailacq and J. Le Rochellec, "The effect of controlled photopigment excitations on pupil aperture," *Ophthalmic & Physiological Optics,* vol. 30, no. 5, pp. 484-491, 2010.

[53] H. Ishikawa, A. Onodera, K. Asakawa, S. Nakadomari and K. Shimizu, "Effects of selective-wavelength block filters on pupillary light reflex under red and blue light stimuli," *Japanese Journal of Ophthalmology,* vol. 56, no. 2, pp. 181-186, 2012.

[54] J. E. Lebensohn and J. Bellows, “The nature of photophobia,” *Archives of Ophthalmology,* vol. 12, no. 3, pp. 380-390, 1934.

[55] B. J. Katz and K. B. Digre, “Diagnosis, pathophysiology, and treatment of photophobia,” *Survey of Ophthalmology,* vol. 61, no. 4, pp. 466-477, 2016.

[56] R. Noseda, V. Kainz, M. Jakubowski, J. J. Gooley, C. B. Saper, K. Digre and R. Burstein, “A neural mechanism for exacerbation of headache by light,” *Nature Neuroscience,* vol. 13, no. 2, pp. 239-245, 2010.

[57] R. N. Hoggan, A. Subhash, S. Blair, K. B. Digre, S. K. Baggaley, J. Gordon, K. C. Brennan, J. E. Warner, A. V. Crum and B. J. Katz, “Thin-film optical notch filter spectacle coatings for the treatment of migraine and photophobia,” *Journal of Clinical Neuroscience,* vol. 28, pp. 71-76, 2016.

[58] S. Hattar, H. W. Liao, M. Takao, D. M. Berson and K. W. Yau, “Melanopsin-containing retinal ganglion cells: architecture, projections, and intrinsic photosensitivity,” *Science,* vol. 295, no. 5557, pp. 1065-1070, 2002.

[59] Z. Melyan, E. E. Tarttelin, J. Bellingham, R. J. Lucas and M. W. Hankins, “Addition of human melanopsin renders mammalian cells photoresponsive,” *Nature,* vol. 433, no. 7027, pp. 741-745, 2005.

[60] L. S. Mure, C. Rieux, S. Hattar and H. M. Cooper, “Melanopsin-dependent nonvisual responses: Evidence for photopigment bistability in vivo,” *Journal of Biological Rhythms,* vol. 22, no. 5, pp. 411-424, 2007.

[61] W. F. Stewart, R. B. Lipton, D. D. Celentano and M. L. Reed, “Prevalence of migraine headache in the United States. Relation to age, income, race, and other sociodemographic factors,” *JAMA,* vol. 267, no. 1, pp. 64-69, 1992.

[62] R. B. Lipton, D. Dodick, R. Sadovsky and et al, “A self-administered screener for migraine in primary care: the ID Migraine validation study,” *Neurology,* vol. 61, no. 3, pp. 375-382, 2003.

[63] W. H. Adams, K. B. Digre, B. C. Patel, R. L. Anderson, J. E. Warner and B. J. Katz, “The Evaluation of Light Sensitivity in Benign Essential Blepharospasm,” *American Journal of Ophthalmology,* vol. 142, no. 1, pp. 82-87, 2006.

[64] M. Hallet, “Blephorospasms: Recent Advances,” *Neurology,* vol. 59, no. 9, pp. 1306-1312, 2002.

[65] R. L. Anderson, B. C. Patel, J. B. Holds and D. R. Jordan, “Blepharospasm: past, present, and future,” *Opthalmic Plastic & Reconstructive Surgery,* vol. 14, no. 5, pp. 305-317, 1998.

[66] M. K. Blackburn, R. D. Lamb, K. B. Digre and et al, “FL-41 tint improves blink frequency, light sensitivity, and functional limitations in patients with benign essential blepharospasm,” *Ophthalmology,* vol. 116, no. 5, pp. 997-1001, 2009.

[67] M. Yap, “The effect of a yellow filter on contrast sensitivity,” *Ophthalmic & Physiological Optics,* vol. 4, no. 3, pp. 227-232, 1984.

[68] J. A. Zuclich, R. D. Glickman and A. R. Menendez, “In situ measurements of lens fluorescence and its interference with visual function,” *Investigative Ophthalmology & Visual Science,* vol. 33, no. 2, pp. 410-415, 1992.

[69] J. Rymer, V. Choh, S. Bharadwai and et al, “The albino chick as a model for studying ocular developmental anomalies, including refractive errors, associated with albinism,” *Experimental Eye Research,* vol. 85, no. 4, pp. 431-442, 2007.

[70] J. S. Leat, R. V. North and H. Bryson, “Do long wavelength pass filters improve low vision performance?,” *Ophthalmic & Physiological Optics,* vol. 10, pp. 219-224, 1990.

[71] S. Zigman, “Vision enhancement using a short wavelength,” *Optometry and Vision Science,* vol. 267, pp. 100-104, 1990.

[72] S. Zigman, “Light filters to improve vision,” *Optometry and Vision Science,* vol. 69, pp. 325-328, 1992.

[73] B. Colligris, H. A. Alkozi and J. Pintor, “Recent developments on dry eye disease treatment compounds,” *Saudi Journal of Ophthalmology,* vol. 28, no. 1, pp. 19-30, 2014.

[74] M. Kaido, I. Toda, T. Oobayashi, M. Kawashima, Y. Katada and K. Tsubota, “Reducing Short-Wavelength Blue Light in Dry Eye Patients with Unstable Tear Film Improves Performance on Tests of Visual Acuity,” *PLoS One,* vol. 11, 2016.

[75] S. M. Blair, P. Kasinadhuni, S. McDaniel and B. J. Katz, “Nanoparticle light filtering method and apparatus”. US Patent US20150168616A1, 15 November 2013.

[76] E. Carlson and S. MacGuffe, “Tinted polarized lenses having selective frequency filtering”. US Patent US9891448B2, 8 August 2014.

[77] M. F. Weber, J. T. Kahl and G. E. Casner, “Circadian rhythm optical film”. US Patent US20150268396A1, 20 March 2014.

[78] A. W. Ishak, J. N. Haddock, W. Kokonaski, D. P. Duston, V. S. Iyer, R. D. Blum, S. P. McGinnis and M. B. Packard, “Photochromic ophthalmic systems that selectively filter specific blue light wavelengths”. US Patent US9377569B2, 20 March 2006.

[79] A. W. ISHAK, S. P. McGinnis, R. D. Blum and M. B. Packard, “High energy visible light filter systems with yellowness index values”. US Patent US8882267B2, 20 March 2006.

[80] A. Ishak, “Rugate optical lens to prevent macular degeneration”. US Patent US20060092374A1, 2 Novmeber 2001.

[81] T. W. Leung, W.-h. R. Li and C.-s. Kee, “Blue-Light Filtering Spectacle Lenses: Optical and Clinical Performances,” *PLoS One,* vol. 12, p. e0169114, 2017.

[82] M. L. McDermott and J. W. Chandler, “Therapeutic uses of contact lenses,” *Survey of Ophthalmology,* vol. 33, no. 5, pp. 381-394, 1989.

[83] F. J. van Kuijk, “Effects of ultraviolet light on the eye: role of protective glasses,” *Environmental Health Perspectives ,* vol. 96, pp. 177-184, 1991.

[84] L. S. Kwok, V. A. Kuznetsov and M. T. Coroneo, “Prevention of the adverse photic effects of peripheral light-focusing using UV-blocking contact lenses,” *Investigative Ophthalmology & Visual Science,* vol. 44, no. 4, pp. 1501-1507, 2003.

[85] J. E. Walsh, J. P. G. Bergmanson, D. Wallace, G. Saldana, H. Dempsey, H. McEvoy and L. M. T. Collum, “Quantification of the ultraviolet radiation (UVR) field in the human eye in vivo using novel instrumentation and the potential benefits of UVR blocking hydrogel contact lens,” *British Journal of Ophthalmology ,* vol. 85, pp. 1080-1085, 2001.

[86] “ACUVUE BRAND CONTACT LENSES,” Johnson & Johnson Vision Care, Inc, [Online]. Available: https://www.acuvue.com/why-contact-lenses/uv-blocking-benefits. [Accessed 13 June 2018].

[87] “Cooper Vision,” Cooper Vision, [Online]. Available: https://coopervision.ca/contact-lenses/sapphire-family/sapphire-toric. [Accessed 13 June 2018].

[88] S. Gause and A. Chauhan, “Nanoparticle-loaded UV-blocking contact lenses,” *Journal of Applied Polymer Science,* vol. 132, no. 37, 2015.

[89] C. Lakkis, K.-Y. Lian, G. Napper and P. M. Kiely, “Infection control guidelines for optometrists 2007,” *Clinical and Experimental Optometry,* vol. 90, no. 6, 2007.

[90] T. G. Smijs and S. Pavel, “Titanium dioxide and zinc oxide nanoparticles in sunscreens: focus on their safety and effectiveness,” *Nanotechnology, Science and Applications,* vol. 4, pp. 95-112, 2011.

[91] R. Asahi, T. Morikawa, T. Ohwaki, K. Aoki and Y. Taga, “Visible-Light Photocatalysis in Nitrogen-Doped Titanium Oxides,” *Science,* vol. 293, no. 5528, pp. 269-271, 2001.

[92] S. Hoang, S. P. Berglund, N. T. Hahn, A. J. Bard and C. B. Mullins, “Enhancing Visible Light Photo-oxidation of Water with TiO2 Nanowire Arrays via Cotreatment with H-2 and NH3: Synergistic Effects between Ti3+ and N,” *Journal of American Chemical Society,* vol. 134, no. 8, pp. 3659-3662, 2012.

[93] A. Caravaca, W. Jones, C. Hardacre and M. Bowker, “H2 production by the photocatalytic reforming of cellulose and raw biomass using Ni, Pd, Pt and Au on titania,” *Proceedings of the Royal Society A: Mathematical, Physical and Engineering Sciences,* vol. 472, p. 20160054, 2016.

[94] J. Wang, N. Zhang, J. Su and L. Guo, “a-Fe2O3 quantum dots: low-cost synthesis and photocatalytic oxygen evolution capabilities,” *RSC Advances,* vol. 6, p. 41060–41066, 2016.

[95] J. Luo, L. J. Cote, V. C. Tung, A. T. L. Tan, P. E. Goins, J. Wu and J. Huang, “Graphene Oxide Nanocolloids,” *Journal of American Chemical Society,* vol. 132, no. 50, pp. 17667-17669, 2010.

[96] Y. Shin, J. Lee, J. Yang, J. Park, S. Kim, Y. Park and H. Lee, “Mass Production of Graphene Quantum Dots by One-Pot Synthesis Directly from Graphite in High Yield,” *Small,* vol. 10, no. 5, pp. 866-870, 2014.

[97] R. Hardman, “A Toxicologic Review of Quantum Dots: Toxicity Depends on Physicochemical and Environmental Factors,” *Environmental Health Perspectives,* vol. 114, no. 2, pp. 165-172, 2006.

[98] Y. Teow, P. V. Asharani, M. P. Hande and S. Valiyaveettil, “Health impact and safety of engineered nanomaterials,” *Chemical Communications,* vol. 47, no. 25, pp. 7025-7038, 2011.

[99] Y. Sun and Y. Xia, “Gold and silver nanoparticles: A class of chromophores with colors tunable in the range from 400 to 750 nm,” *Analyst,* vol. 128, pp. 686-691, 2003.

[100] J. Boken, P. Khurana, S. Thatai, D. Kumar and S. Prasad, “Plasmonic nanoparticles and their analytical applications: A review,” *Applied Spectroscopy Reviews,* vol. 52, no. 9, pp. 774-820, 2017.

[101] G. Mie, “Contributions on the optics of turbid media, particularly colloidal metal solutions,” *Annals of Physics,* vol. 25, no. 3, pp. 377-445, 1908.

[102] M. Rycenga, C. M. Cobley, J. Zeng, W. Li, C. H. Moran, Q. Zhang, D. Qin and Y. Xia, “Controlling the Synthesis and Assembly of Silver Nanostructures for Plasmonic Applications,” *Chemical Reviews,* vol. 111, no. 6, pp. 3669-3712, 2011.

[103] T. P. Ontanicar, D. DeJarnette, Y. Hewakuruppu and R. A. Taylor, “Filtering light with nanoparticles: a review of optically selective particles and applications,” *Advances in Optics and Photonics,* vol. 8, no. 3, pp. 541-585, 2016.

[104] G. Lilley, M. Messner and K. Unterrainer, “Improving the quality factor of the localized surface plasmon resonance,” *Optical Materials Express,* vol. 5, no. 10, pp. 2112-2120, 2015.

[105] M. Perner, P. Bost, U. Lemmer, G. von Plessen, J. Feldmann, U. Becker, M. Mennig, M. Schmitt and H. Schmitt, “Optically Induced Damping of the Surface Plasmon Resonance in Gold Colloids,” *Physical Review Letters,* vol. 78, no. 11, pp. 2192-2195, 1997.

[106] H. Wang, F. Tam, N. K. Grady and N. J. Halas, “Cu Nanoshells: Effects of Interband Transitions on the Nanoparticle Plasmon Resonance,” *The Journal of Physical Chemistry B,* vol. 109, no. 39, pp. 18218-18222, 2005.

[107] S.-W. Baek, J. Noh, C.-H. Lee, B. Kim, M.-K. Seo and J.-Y. Lee, “Plasmonic Forward Scattering Effect in Organic Solar Cells: A Powerful Optical Engineering Method,” *Scientific Reports,* vol. 3, p. 1726, 2013.

[108] K.-C. Lee, S.-J. Lin, C.-H. Lin, C.-S. Tsai and Y.-J. Lu, “Size effect of Ag nanoparticles on surface plasmon resonance,” *Surface and Coatings Technology,* vol. 202, no. 22-23, pp. 5339-5342, 2008.

[109] J. Zeng, S. Roberts and Y. Xia, “Nanocrystal-Based Time–Temperature Indicators,” *Chemistry - A European Journal,* vol. 16, no. 42, 2010.

[110] S.-H. Jeong, H. Choi, J. Y. Kim and T.-W. Lee, “Silver-Based Nanoparticles for Surface Plasmon Resonance in Organic Optoelectronics,” *Particle & Particle Systems Characterization,* vol. 32, no. 2, 2014.

[111] D. Paramelle, A. Sadovoy, S. Gorelik, P. Free, J. Hobley and D. G. Fernig, “A rapid method to estimate the concentration of citrate capped silver nanoparticles from UV-visible light spectra,” *Analyst,* vol. 139, pp. 4855-4861, 2014.

[112] F. J. Beck, A. Polman and K. R. Catchpole, “Tunable light trapping for solar cells using localized surface plasmons,” *Journal of Applied Physics,* vol. 105, p. 114310, 2009.

[113] S. Liu, M. D. Regulacio, S. Y. Tee, Y. W. Khin, P. C. Teng, L. D. Koh, G. Guan and M.-Y. Han, “Preparation, Functionality, and Application of Metal Oxide-coated Noble Metal Nanoparticles,” *The Chemical Record,* vol. 16, no. 4, pp. 1965-1990, 2016.

[114] C. Hanske, M. N. Sanz-Ortiz and L. M. Liz-Marzan, “Silica-Coated Plasmonic Metal Nanoparticles in Action,” *Advanced Materials,* vol. 0, no. 0, p. 1707003, 2018.

[115] S. Liu and M.-Y. Han, “Silica-Coated Metal Nanoparticles,” *Chemistry - An Asian Journal,* vol. 5, no. 1, 2009.

[116] A. Guerrero-Martinez, J. Perez-Juste and L. M. Liz-Marzan, “Recent progress on silica coating of nanoparticles and related nanomaterials,” *Advanced Materials,* vol. 22, no. 11, pp. 1182-1195, 2010.

[117] S. Biggs and P. Mulvaney, “Measurement of the forces between gold surfaces in water by atomic force microscopy,” *The Journal of Chemical Physics,* vol. 100, 1994.

[118] A. O. Pinchuk, “Size-Dependent Hamaker Constant for Silver Nanoparticles,” *The Journal of Physical Chemistry C,* vol. 116, no. 37, p. 20099−20102, 2012.

[119] J. L. Montano-Priede, O. Pena-Rodriguez and U. Pal, “Near-Electric-Field Tuned Plasmonic Au@SiO2 and Ag@SiO2 Nanoparticles for Efficient Utilization in Luminescence Enhancement and Surface-Enhanced Spectroscopy,” *The Journal of Physical Chemistry C,* vol. 121, no. 41, pp. 23062-23071, 2017.

[120] M. P. Brandon, D. M. Ledwith and J. M. Kelly, “Preparation of saline-stable, silica-coated triangular silver nanoplates of use for optical sensing,” *Journal of Colloid and Interface Science,* vol. 415, pp. 77-84, 2014.

[121] K. L. Wustholz, A. I. Henry, J. M. McMahon, R. G. Freeman, N. Valley, M. E. Piotti, M. J. Natan, G. C. Schatz and R. P. Van Duyne, “Structure-activity relationships in gold nanoparticle dimers and trimers for surface-enhanced Raman spectroscopy,” *Journal of the American Chemical Society,* vol. 132, no. 31, pp. 10903-10910, 2010.

[122] P. Botella, I. Ortega, M. Quesada, R. F. Madrigal, C. Muniesa, A. Fimia, E. Fernandez and A. Corma, “Multifunctional hybrid materials for combined photo and chemotherapy of cancer,” *Dalton Transactions,* vol. 41, no. 31, p. 9286, 2012.

[123] G. A. Sotiriou, T. Sannomiya, A. Teleki, F. Krumeich, J. Voros and S. E. Pratsinis, “Non-toxic dry-coated nanosilver for plasmonic biosensors,” *Advanced Functional Materials,* vol. 20, no. 24, pp. 4250-4257, 2010.

[124] Q. Zeng, Y. Zhang, W. Ji, W. Ye, Y. Jiang and J. Song, “Inhibitation of cellular toxicity of gold nanoparticles by surface encapsulation of silica shell for hepatocarcinoma cell application,” *ACS Applied Material Interfaces,* vol. 6, no. 21, pp. 19327-19335, 2014.

[125] S. Liu, Z. Zhang, Y. Wang, F. W. Wang and M. Y. Han, “Surface-functionalized silica-coated gold nanoparticles and their bioapplications,” *Talanta,* vol. 67, pp. 456-461, 2005.

[126] S. Liu, Z. Zhang and M. Y. Han, “Gram-Scale Synthesis and Biofunctionalization of Silica-Coated Silver Nanoparticles for Fast Colorimetric DNA Detection,” *Anal. Chem,* vol. 77, pp. 2595-2600, 2005.

[127] P. K. Jal, S. Patel and B. K. Mishra, "Chemical modification of silica surface by immobilization of functional groups for extractive concentration of metal ions," *Talanta,* vol. 62, no. 5, pp. 1005-1028, 2004.

[128] Y. Yin, Z.-Y. Li, Z. Zhong, B. Gates, Y. Xia and S. Venkateswaran, "Synthesis and characterization of stable aqueous dispersions of silver nanoparticles through the Tollens process," *J. Mater. Chem,* vol. 12, pp. 522-527, 2002.

[129] P. C. Lee and D. Meisel, "Adsorption and surface-enhanced Raman of dyes on silver and gold sols," *J. Phys. Chem,* vol. 86, no. 17, pp. 3391-3395, 1982.

[130] Y. Sun and Y. Xia, "Shape-Controlled Synthesis of Gold and Silver Nanoparticles," *Science,* vol. 298, pp. 2176-2179, 2002.

[131] Q. Zhang, W. Li, C. Moran, J. Zeng, J. Chen, L. P. Wen and Y. Xia, "Seed-mediated synthesis of Ag nanocubes with controllable edge lengths in the range of 30-200 nm and comparison of their optical properties," *J. Am. Chem. Soc,* vol. 132, no. 32, pp. 11372-11378, 2010.

[132] R. Jin, Y. C. Cao, E. Hao, G. S. Metraux, G. C. Schatz and C. A. Mirkin, "Controlling anisotropic nanoparticle growth through plasmon excitation," *Nature,* vol. 425, no. 6957, pp. 487-490, 2003.

[133] Y. Wang, Y. Zheng, C. Z. Huang and Y. Xia, "Synthesis of Ag Nanocubes 18–32 nm in Edge Length: The Effects of Polyol on Reduction Kinetics, Size Control, and Reproducibility," *J. Am. Chem. Soc.,* vol. 135, no. 5, pp. 1941-1951, 2013.

[134] Q. Zhang, W. Li, L.-P. Wen, J. Chen and Y. Xia, "Facile Synthesis of Ag Nanocubes of 30 to 70 nm in Edge Length with CF3COOAg as a Precursor," *Chemistry,* vol. 16, no. 33, pp. 10234-10239, 2010.

[135] S. H. Im, Y. T. Lee, B. Wiley and Y. Xia, "Large-Scale Synthesis of Silver Nanocubes: The Role of HCl Promoting Cubic Perfection and Monodispersity," *Angew. Chem. Int. Ed.,* vol. 44, pp. 2154-2157, 2005.

[136] A. Ruditskiy and Y. Xia, "Toward the Synthesis of Sub-15 nm Ag Nanocubes with Sharp Corners and Edges: The Roles of Heterogeneous Nucleation and Surface Capping," *J. Am. Chem. Soc.,* vol. 138, no. 9, pp. 3161-3167, 2016.

[137] X. Xia, J. Zeng, L. K. Oetjen, Q. Li and Y. Xia, "Quantitative Analysis of the Role Played by Poly(vinylpyrrolidone) in Seed-Mediated Growth of Ag Nanocrystals," *J. Am. Chem. Soc.,* vol. 134, no. 3, pp. 1793-1801, 2012.

[138] W. Li and Y. Xia, "Facile Synthesis of Gold Octahedra by Direct Reduction of HAuCl4 in an Aqueous Solution," *Chem. Asian J,* vol. 5, pp. 1312-1316, 2010.

[139] Y. Wang, D. Wan, S. Xie, X. Xia, C. Z. Huang and Y. Xia, "Synthesis of Silver Octahedra with Controlled Sizes and Optical Properties via Seed-Mediated Growth," *ACS Nano,* vol. 7, no. 5, pp. 4586-4594, 2013.

[140] C. Graf, D. L. J. Vossen, A. Imhof and A. van Blaaderen, "A General Method To Coat Colloidal Particles with Silica," *Langmuir,* vol. 19, no. 17, pp. 6693-6700, 2003.

[141] M. A. Green, Y. Hishikawa, E. D. Dunlop, D. H. Levi, J. Hohl-Ebinger and A. W. Ho-Baillie, "Solar cell efficiency tables (version 51)," *Progress in Photovoltaics: Research and Applications,* vol. 26, no. 1, pp. 3-12, 2017.

[142] T. Leshuk, H. Krishnakumar, D. d. O. Livera and F. Gu, "Floating Photocatalysts for Passive Degradation of Naphthenic Acids in Oil Sands Process-Affected Water," *Water,* vol. 10, no. 2, 2018.

[143] "Current Readings," UW Weather Station, [Online]. Available: http://weather.uwaterloo.ca/. [Accessed 14 May 2014].

[144] K. Esumi and M. Oyama, "Simultaneous Adsorption of Poly(vinylpyrrolidone) and Cationic Surfactant from Their Mixed Solutions on Silica," *Langmuir,* vol. 9, pp. 2020-2023, 1993.

[145] N. Grillet, D. Manchon, E. Cottancin, C. Bertorelle, M. Broyer, J. Lerme and M. Pellarin, "Photo-Oxidation of Individual Silver Nanoparticles: A Real-Time Tracking of Optical and Morphological Changes," *J. Phys. Chem. C,* vol. 117, no. 5, pp. 2274-2282, 2013.

Appendices

Appendix A Histogram showing the diameter distribution of octahedra AgNPs synthesized under optimized polyol synthesis conditions

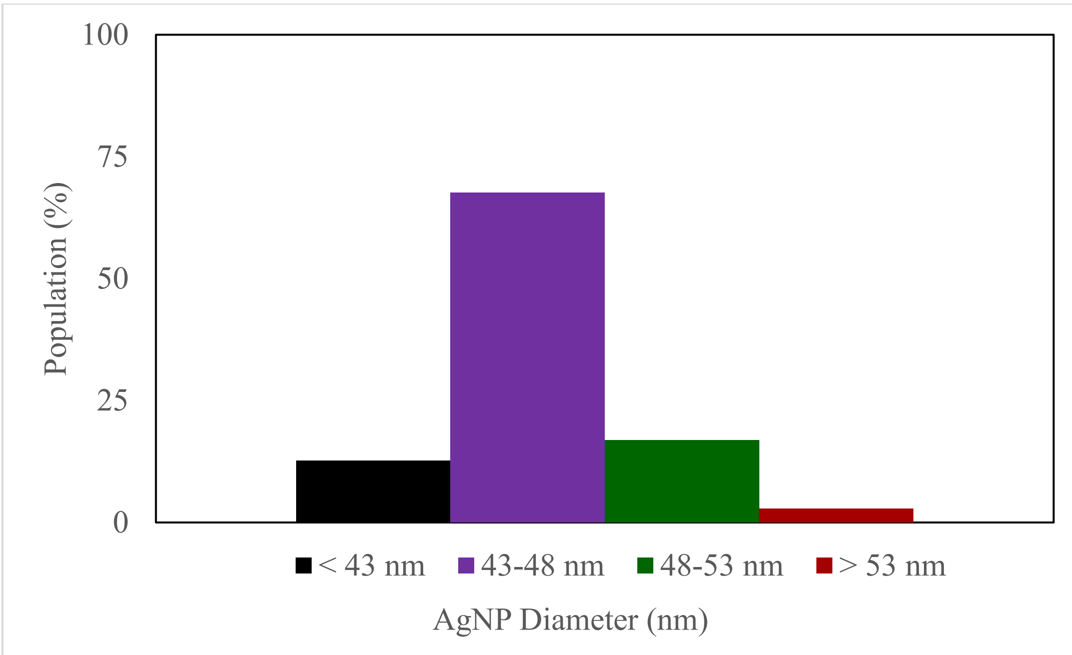

Figure 19. Histogram showing the diameter distribution of octahedra AgNPs synthesized after 120 minutes under optimized polyol synthesis conditions.

Appendix B Reproducibility of cubic and octahedra AgNPs under optimized polyol synthesis conditions

Table 17. Reproducibility of cubic and octahedra AgNPs under optimized polyol synthesis conditions.

	Time (min)						
	30	45	60	75	90	105	120
	Octahedra						
Replicate 1	405 (29)	406 (28)	413 (30)	425-426 (36)	435 (34)	440 (35)	441 (35)
Replicate 2	407 (30)	406 (28)	415 (32)	426 (36)	436 (36)	442 (36)	444 (37)
Replicate 3	408 (30)	407 (29)	416 (31)	427 (36)	438 (38)	441 (38)	444 (37)
Replicate 4	410 (31)	408 28	410 (28)	420 (37)	433 (38)	441 (36)	443 (36)
Replicate 5	408 (34)	421 (39)	433 (43)	445 (44)	446 (45)	447 (45)	445 (42)
Replicate 6	407 (47)	409 (43)	409 (38)	410 (37)	415 (36)	423 (39)	435 (42)
Replicate 7	406 (46)	405 (54)	410 (37)	422 (38)	434 (41)	442 (42)	446 (39)
	Cubes						
Replicate 1	403-405 (101)	411 (42)	413 (41)	418 (44)	422 (40)	425 (50)	429 (40)
Replicate 2	412 (47)	417 (48)	423 (46)	429 (53)	434 (55)	434 (48)	430 (49)
Replicate 3	415 (47)	419 (53)	421 (44)	423-424 (45)	425-426 (61)	429 (55)	431 (48)
Replicate 4	418 (54)	421 (47)	423 (54)	426 (45)	430-431 (49)	433 (44)	436-437 (42)
Replicate 5	409 (197)	412 (91)	416 (60)	420 (56)	425 (68)	431 (42)	--
Replicate 6	407 (67)	413-414 (52)	417 (50)	420 (49)	423 (53)	426 (50)	429-430 (49)
Replicate 7	408 (43)	413 (39)	417 (43)	422 (44)	428 (40)	--	--

Appendix C TEM images of silica-coated octahedra AgNPs

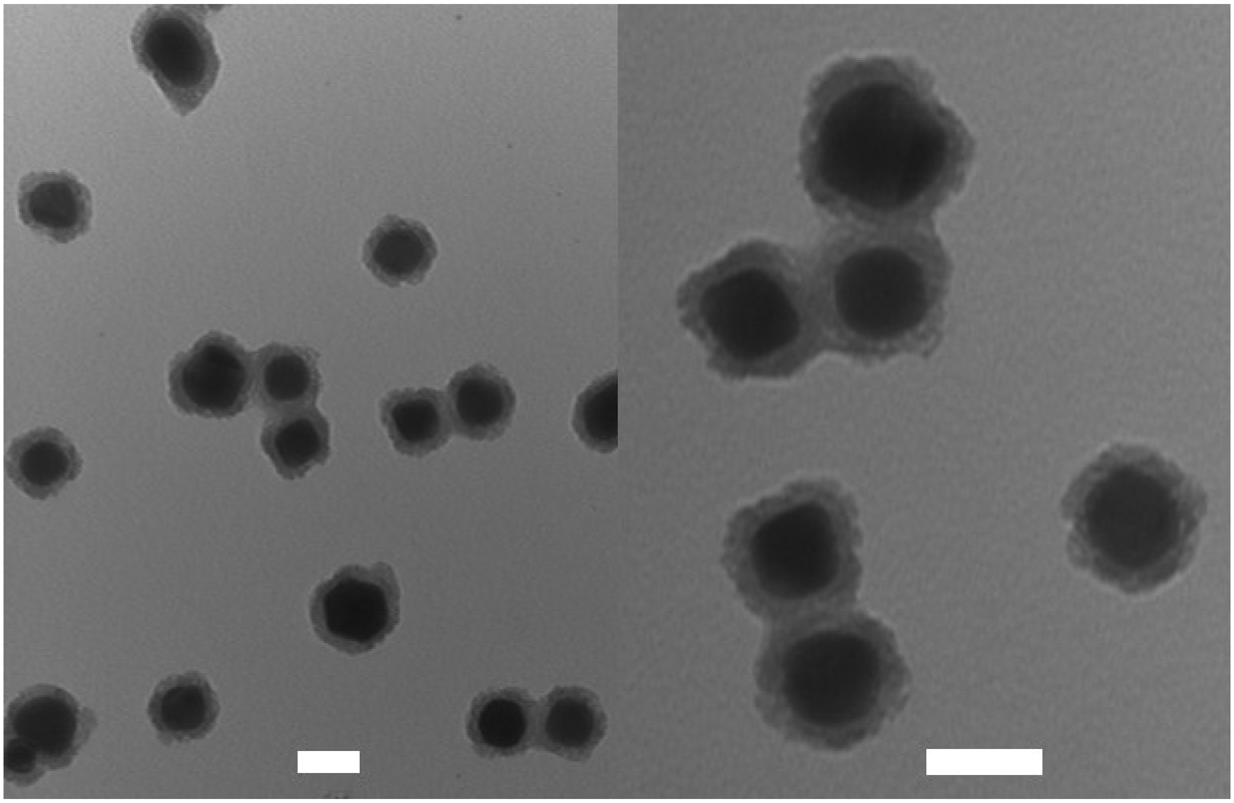

Figure 20. TEM images of octahedra NPs after silica coating (and washing). Scalebars represent 50 nm.

Appendix D Light blockage determination

Light blockage (%) at specific wavelengths is a function of the optical density (OD), as shown in Equation 3:

$$Light\ Blocked\ \% = (1 - 10^{-OD}) * 100\%$$

Equation 3. Light blockage

Appendix E Outdoor solar irradiation on May 14, 2018

Table 18. Outdoor solar irradiation on May 14, 2018. [143]

Time	Incoming Radiation (W/m^2)
10:00 AM	556.4
10:15 AM	586.2
10:30 AM	549.4
10:45 AM	677.1
11:00 AM	673.8
11:15 AM	629.8
11:30 AM	659.6
11:45 AM	641.2
12:00 PM	557.4
12:15 PM	570.0
12:30 PM	832.8
12:45 PM	678.5
1:00 PM	446.9
1:15 PM	456.7
1:30 PM	263.8
1:45 PM	238.3
2:00 PM	359.9
2:15 PM	721.7
2:30 PM	471.5
2:45 PM	572.2
3:00 PM	789.3
3:15 PM	568.8
3:30 PM	759.0
3:45 PM	751.9
4:00 PM	436.1
4:15 PM	597.8

Appendix F FWHM of autoclaved lens

For this lens, the FWHM was determined using double the HWHM value (on the right half side of the LSPR peak).

Appendix G Mass of Ag per lens

Concentration of Ag in NP-monomer mixture = 88.58 mg/L (determined by ICP analysis)

Volume of NP-monomer mixture required per lens = 140 uL

Mass of Ag per lens = 88.58 mg/L * 140 uL = 12.401 ug